Preliminary Report

Modeling of River Hydrodynamics with D-Flow Flexible Mesh and 3Di

Case Study of the river Elbe

F. Fennis B.Sc.

Faculty of Civil Engineering & EEMCS · Delft University of Technology

Modeling of River Hydrodynamics with D-Flow Flexible Mesh and 3Di

Case Study of the river Elbe

Preliminary Report

F. Fennis B.Sc.

Head of department Applied Mathematics: prof.dr.ir. C. Vuik

Head of department Hydraulic Engineering: prof.dr.ir. W.S.J. Uijttewaal

Supervisor: dr.ir. J.L. Korving

Faculty of Civil Engineering & EEMCS · Delft University of Technology

Contents

List of Figures vi

Nomenclature vii

1 Introduction 1

1.1 Problem description 1

1.2 Research Methodology 2

2 Description of the mathematical model 3

2.1 Navier-Stokes equations 3

2.1.1 Conservation of mass 4

2.1.2 Conservation of momentum 4

2.2 Grid generation 5

2.2.1 Structured grid 6

2.2.2 Unstructured grid 7

3 Shallow water equations 9

3.1 Reynolds averaged Navier-Stokes equations 9

3.2 Boundary conditions 10

3.3 Scaling 11

3.4 2D shallow-water equations 12

3.5 Assumptions 13

3.6 Difference in processes in 3Di and Flexible Mesh 16

4 D-Flow Flexible Mesh **19**
4.1 Grid generation . . . 19
4.1.1 Connectivity . . . 21
4.1.2 Bed geometry . . . 22
4.2 Discretisation of shallow water equations . . . 24
4.2.1 Spatial discretisation . . . 24
4.2.2 Time discretisation . . . 26

5 3Di **29**
5.1 Quadtrees . . . 29
5.2 Subgrid . . . 30
5.2.1 Integration of the grids . . . 32
5.3 Discretisation of the shallow water equations . . . 34
5.3.1 Spatial discretisation . . . 35
5.3.2 Time discretisation . . . 40

6 Description of the problem **43**
6.1 Research questions . . . 43
6.2 Test models . . . 44
6.2.1 Straight channel with rectangular cross section . . . 44
6.2.2 U-bend . . . 45
6.2.3 Straight channel with trapezoidal cross section . . . 46
6.2.4 River Elbe . . . 46

References **48**

A Derivation of mass and momentum equations **51**
A.1 Conservation of mass . . . 51
A.2 Conservation of momentum . . . 52

B Derivation of the shallow water equations **55**
B.1 RANS equations . . . 55
B.2 Scaling . . . 56
B.3 Depth integration . . . 58

List of Figures

2.1 Coordinate system . . . 3
2.2 Grid cell definitions . . . 5
2.3 Admitted and nonadmitted cells . . . 6
2.4 Layout of grid points in a structured grid . . . 6
2.5 Sub-grid with quadtrees . . . 7
2.6 Unstructured grid . . . 7

3.1 Secondary flow in a bend . . . 15
3.2 Helical flow (Jirka and Uijttewaal, 2004) . . . 15

4.1 Net (domain discretisation) . . . 20
4.2 Perfect orthogonality (left) and perfect smoothness (right) . . . 20
4.3 Small flowlinks . . . 21
4.4 Behaviour of the flow when a flowlink misses . . . 21
4.5 Example of notations (Deltares, 2015) . . . 22
4.6 Flow area A_{uj} and face-based water depth h_{uj} (Deltares, 2015) . . . 23
4.7 Control volumes of triangular grid (Kernkamp et al., 2011) . . . 25

5.1 Grid cell numbering in two layers . . . 29
5.2 Grid cell numbering . . . 30
5.3 Coarse cell with sub-grid . . . 31
5.4 Coarse grid sub-domains (Stelling, 2012) . . . 31
5.5 Discharges for momentum transport (Stelling, 2012) . . . 36

6.1 Straight channel with rectangular cross section . . . 45
6.2 U-bend . . . 45
6.3 Straight channel with trapezoidal cross section . . . 46

6.4 River Elbe 47
A.1 Fluid particle 51

Nomenclature

Latin Symbols

g	Gravitational acceleration	$[ms^{-2}]$
t	Time	$[s]$
u	Velocity x-direction	$[ms^{-1}]$
v	Velocity y-direction	$[ms^{-1}]$
w	Velocity z-direction	$[ms^{-1}]$
A	Cross sectional area	$[m^2]$
A_{uj}	Flow area	$[m^2]$
bob	Face-based bed levels	$[m]$
C	Chezy number	$[m^{1/2}s^{-1}]$
c_f	Friction coefficient	$[-]$
f	Coriolis parameter	$[rads^{-1}]$
Fr	Froude number	$[-]$
$\overline{f_{\text{vis}}}$	Viscous force	$[kgm^{-2}s^{-2}]$
h	Water depth	$[m]$
h_{uj}	Face-based water depth	$[m]$
i	Bed slope	$[-]$
n	Manning coefficient	$[m^{-1/3}s]$
P	Wet perimeter	$[m]$
p	Pressure	$[Pa]$
p_a	Atmosphere pressure	$[Pa]$
Q	Discharge	$[m^3s{-}1]$

R	Hydraulic radius	$[m]$
Re	Reynolds number	$[-]$
Ro	Rossby number	$[-]$
S_f	Friction slope	$[-]$
∇^S	Symmetric operator	$[-]$
T	Lateral stresses	$[Pa]$
V	Volume	$[m^3]$
w_{uj}	Face width	$[m]$
z_b	Bottom level	$[m]$
z_i	Node-based bed levels	$[m]$

Greek Symbols

ϵ	Roughness height	$[m]$
ζ	Water level	$[m]$
μ	Dynamic viscosity	$[kgs^{-1}m^{-1}]$
ν	Kinematic viscosity	$[kgs^{-1}m^{-1}]$
ρ	Density	$[kgm^{-3}]$
τ	Shear stress	$[Pa]$
ϕ	Latitude	$[-]$
Ω	Rotation rate of the Earth	$[rads^{-1}]$

Other Symbols

$\mathcal{I}$	Set that contains mesh nodes
$\mathcal{J}$	Set that contains vertical faces

Chapter 1

Introduction

In the Netherlands it is of importance to know how the water is behaving in rivers due to the danger it can bring with it. Present day we are still building structures in rivers or adjusting it in some way, which results in changes in the hydrodynamics and morphology. The modeling of rivers is therefore necessary to get a better understanding of how the river responses to these adjustments. For the last decades computer programs have been made that are able to model rivers. Even now, new programs are being made that are more precise in predicting the consequences of adjustments. Two of these new programs are D-Flow Flexible Mesh (FM) and 3Di. Whereas the first is especially designed to model rivers and other flows, the latter is mostly used in the sector Watermanagement at this moment. Simulations with 3Di can for example show the effects of flooding in a whole city, but it is not frequently used to model the hydrodynamics of rivers.

1.1 Problem description

One of the main differences between these programs is the mesh generation. 3Di generates a grid based on the sub-grid method with quadtrees, while Flexible Mesh works with an unstructured grid that combines the curvilinear grid and triangles. Both kind of grids are not often used in river models, which distinguish these tools from others. From a mathematical point of view these differences between the grids are very interesting. Different grids might lead to dissimilar results and the question would be which of these grids produces a more realistic prediction in what situation.

Even though the programs are new, the grids they use are not. The advantage of these grids is that there is the possibility to refine your grid at certain points without having this refinement over the whole model area. As a result, the computational time is much less than when the whole grid has to be refined. Studies of the refinement of these grids on rivers have been done by Hagen (2014) for Flexible Mesh and Stelling (2012) for 3Di. These studies did not include the transition from a coarse to finer grid in one model. The transition can result in errors that will not be there when the grid is not refined locally. Consequences might be that the results are not quite reliable at these local areas.

Looking at the hydrodynamics it is important that properties like turbulence, diffusivity etc. are processed as best as possible. Hence, the physical aspects should make sense in the model. How well these aspects are modeled can also depend on the type of grid that is used, which brings us back to the previous part. It can be hard to model this, hence, in existing programs some values that are used are physically not realistic even though the result is. However, in that case the model is not suitable for other situations or predicting in a precise way what can happen in the future. Since both Flexible Mesh and 3Di are new programs it is not known how well this is done in each program.

1.2 Research Methodology

This preliminary report contains the literature study that is done in order to specify the aim of this research. Chapter 2 gives a description of the mathematical model. It introduces the equations that are used and describes shortly about the generation of grids. In the third chapter the derivation of the shallow-water equations is done and all assumptions that are used will be discussed. After this a closer look is taken into the program Flexible Mesh. It is described how the grid is generated and how the equations are discretised and solved. In Chapter 6 the same is done except for the program 3Di. This reports ends with describing the research questions and stating some test cases.

Chapter 2

Description of the mathematical model

The starting point of modeling rivers are the Navier-Stokes equations, which describe the evolution of a fluid. The shallow water equations that are used in the programs 3Di and D-Flow Flexible Mesh are derived from the NS equations, which are treated in this chapter. Another important point to introduce is grid generation. Besides the NS equations also a short introduction on different mesh types is given.

2.1 Navier-Stokes equations

The Navier-Stokes equations govern the motion of a viscid fluid and describe the conservation of mass and momentum. In the next subsections both conservations are given. The equations are given for a Cartesian coordinate system. Figure 2.1 shows the coordinate system and the boundaries in the z-direction with ζ the surface elevation above reference plane (dotted lines) and z_b the bottom level above reference plane.

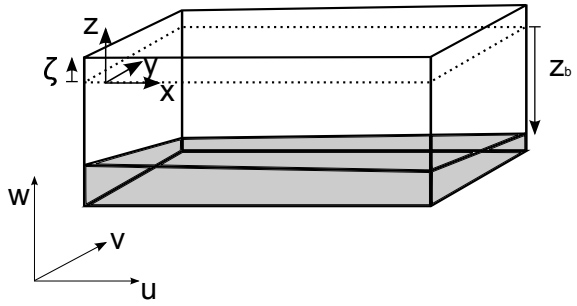

Figure 2.1: Coordinate system

2.1.1 Conservation of mass

The basic point for the derivation of the mass-conservation equation is a mass balance for a fluid particle, given below.

Rate of change of mass in fluid particle = Ingoing flux of mass - Outgoing flux of mass

Using this mass balance leads to the continuity equation for a compressible fluid (2.1). In Appendix A a full derivation of the mass-continuity equation can be found.

$$\frac{\partial \rho}{\partial t} + \frac{\partial \rho u}{\partial x} + \frac{\partial \rho v}{\partial y} + \frac{\partial \rho w}{\partial z} = 0 \tag{2.1}$$

In the case of water it is usually assumed that the fluid is incompressible, hence, has a constant density. According to Vreugdenhil (1994) the only point where you have to use the actual density is at the gravitational acceleration, since density variations are important there. This is called the Boussinesq approximation and results in the continuity equation for an incompressible fluid.

$$\frac{\partial u}{\partial x} + \frac{\partial v}{\partial y} + \frac{\partial w}{\partial z} = 0 \tag{2.2}$$

2.1.2 Conservation of momentum

The basic of the momentum equations is the second law of Newton. In Appendix A a full derivation of the momentum equations can be found with starting point Newton's second law. The general form of the momentum equations is as follows (Ji, 2008),

$$\rho \frac{D\mathbf{v}}{Dt} = \frac{\partial \rho \mathbf{v}}{\partial t} + \nabla \cdot (\rho \mathbf{v}\mathbf{v}) = \rho \mathbf{g} - \nabla p + \overline{f_{\text{vis}}}. \tag{2.3}$$

Beside the absence of some external forces in the above equation, the viscous force is not yet defined. Water is known as an Newtonian fluid, which means that the stresses are linear proportional to the rate of deformation (Ji, 2008). Together with the Boussinesq approximation these viscous forces can be written as

$$\overline{f_{\text{vis}}} = \nabla \cdot \boldsymbol{\tau} \tag{2.4}$$

where the water shear stress is expressed as

$$\begin{aligned} \tau_{xx} &= 2\mu \frac{\partial u}{\partial x} & \tau_{xy} &= \tau_{yx} = \mu \left(\frac{\partial u}{\partial y} + \frac{\partial v}{\partial x} \right) \\ \tau_{yy} &= 2\mu \frac{\partial v}{\partial y} & \tau_{xz} &= \tau_{zx} = \mu \left(\frac{\partial u}{\partial z} + \frac{\partial w}{\partial x} \right) \\ \tau_{zz} &= 2\mu \frac{\partial w}{\partial z} & \tau_{zy} &= \tau_{yz} = \mu \left(\frac{\partial w}{\partial y} + \frac{\partial v}{\partial z} \right) \end{aligned} \tag{2.5}$$

with μ the dynamic viscosity, and where the first subscript denotes the plane on which the stress are working and the second the direction on which the stress works. Substituting expression (2.4) for the viscous forces and considering the Coriolis effect Equation 2.3 transforms in the full set of momentum equations in 3 dimensions.

$$\frac{\partial \rho u}{\partial t} + \frac{\partial \rho u^2}{\partial x} + \frac{\partial \rho uv}{\partial y} + \frac{\partial \rho uw}{\partial z} = -\frac{\partial p}{\partial x} + \rho f v + \left[\frac{\partial \tau_{xx}}{\partial x} + \frac{\partial \tau_{yx}}{\partial y} + \frac{\partial \tau_{zx}}{\partial z}\right] \tag{2.6}$$

$$\frac{\partial \rho v}{\partial t} + \frac{\partial \rho vu}{\partial x} + \frac{\partial \rho v^2}{\partial y} + \frac{\partial \rho vw}{\partial z} = -\frac{\partial p}{\partial y} - \rho f u + \left[\frac{\partial \tau_{xy}}{\partial x} + \frac{\partial \tau_{yy}}{\partial y} + \frac{\partial \tau_{zy}}{\partial z}\right] \tag{2.7}$$

$$\frac{\partial \rho w}{\partial t} + \frac{\partial \rho wu}{\partial x} + \frac{\partial \rho wv}{\partial y} + \frac{\partial \rho w^2}{\partial z} = -\frac{\partial p}{\partial z} - \rho g + \left[\frac{\partial \tau_{xz}}{\partial x} + \frac{\partial \tau_{yz}}{\partial y} + \frac{\partial \tau_{zz}}{\partial z}\right] \tag{2.8}$$

with $f = 2\Omega \sin \phi$ the Coriolis parameter. Ω is the angular velocity of rotation of the Earth and ϕ represents the latitude in degrees. In order to solve the equations, boundary conditions are needed. However, the equations are simplified in Chapter 3 which means that the boundary conditions are needed for the simplified equations. Hence, in Chapter 3 the boundary conditions are given for the simplified equations.

2.2 Grid generation

One of the basic steps of creating a numerical model is the generation of a grid (or mesh) of the area that one is interested in. A grid consists of grid cells that can have various forms. The simplest form is a triangular cell in two-dimensional volumes and a tetrahedral cell in three-dimensional volumes (Liseikin, 2004). This is due to their pertinence to all sorts of domain structures. Figure 2.2 displays these grid cells as an example for the definitions.

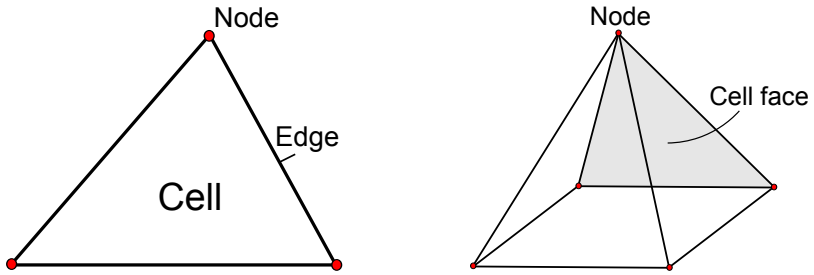

(a) 2-dimensional (b) 3-dimensional

Figure 2.2: Grid cell definitions

It is assumed that the grid cells do not intersect each other. Hence, there cannot be a node of one cell lying in the middle of another cell. When also each node of a cell is either the same node of another cell or belongs to the boundary it is called an admitted intersection. Figure 2.3 displays both admitted and nonadmitted intersections. Number 2 and 3 show a node that is on the edge of another cell. This node is known as a hanging node. When a grid is locally refined it is possible that these hanging nodes occur.

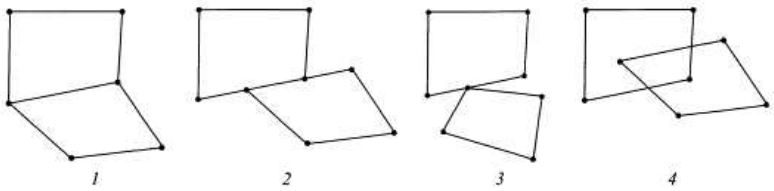

Figure 2.3: Admitted (1) and nonadmitted (2, 3, 4) intersections of neighboring quadrilateral cells (Liseikin, 2004)

Another important point is the grid organization. In order to form and solve the discretized equations that originate from the differential equations, it should be known where the neighboring points and cells are. Some organization is needed for this. The generation of grids can be done in multiple ways. The two fundamental classes are the structured and unstructured grid generation, both are discussed below.

2.2.1 Structured grid

A structured grid (looking in 2D) can consist of a rectangular or curvilinear grid. The left grid of Figure 2.4 shows how a curvilinear grid looks and the right a rectangular grid. Note, this figure displays the transformation of a grid from the physical to the logical space, which is done to solve the model in an easier way. With a structured grid one has an ordered layout of grid points. All the cells are arranged and the location of each cell is known in a way given in Figure 2.4. Due to this arrangement of the cells the computational time is faster compared to an unstructured grid, since finding the value of each cell is much easier. However, looking at modeling rivers, a rectangular grid is often not the best option. The kind of grid is not able to follow the geometry of a river. The result would be a river with a stairway land boundary. So, usually a curvilinear grid is used. Delft 3D Flow uses this grid for example.

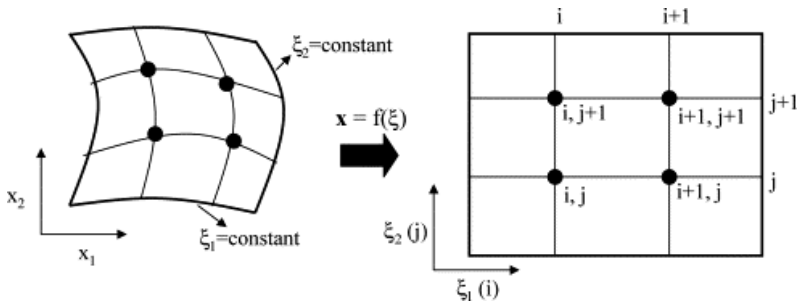

Figure 2.4: Layout of grid points in a structured grid (Chatterjee, 2004)

3Di uses a sub-grid method that is arranged as stated by quadtrees (Stelling, 2012), see Figure 2.5. It can be seen that this method consist of squares in different sizes, where a larger square can be divided into quarters. Hence, a rectangular grid is used even though it is known this is not the best option for rivers. In Chapter 4 this method will be explained in detail.

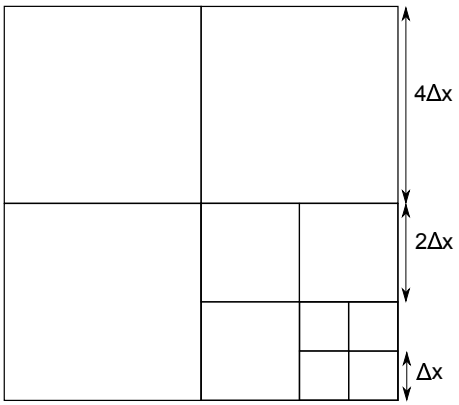

Figure 2.5: Sub-grid with quadtrees

2.2.2 Unstructured grid

Usually, an unstructured grid consist of triangles. However, also other geometric forms are possible. These triangles have the ability to take complex geometries into account. The disadvantages if one uses only triangles, are that the computational time is higher and it uses more memory. The advantage of a structured grid where the location of each cell is known is not there for the triangular grid. The information of the location has to be kept in a table, which uses more memory, and finding the right cells is time consuming.

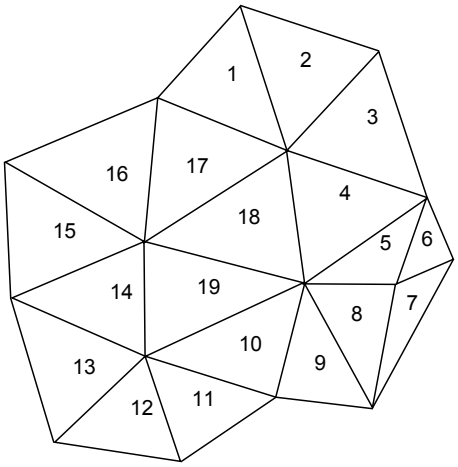

Figure 2.6: Unstructured grid

D-Flow Flexible Mesh uses a combination of triangles and a curvilinear grid (Deltares, 2015), which is sometimes called a hybrid grid since it uses both structured as unstructured grids. When there are complex geometries present in a river (or somewhere else), the triangles can be used to model this far more accurate than when one uses only a curvilinear grid. Where the geometry is less complex the curvilinear grid can be used which has the advantage of a faster computational time and using less memory than working with only a triangular grid. A more detailed explanation is given in Chapter 3 for this type of grid.

Chapter 3

Shallow water equations

Both D-Flow Flexible Mesh and 3Di work with the 2-dimensional depth-averaged equations, also called the 2D Saint-Venant equations or shallow water equations. They originate from the Navier-Stokes equations. The latter are however not easy to solve. Thus, most of the time, simplifications are used based on various assumptions. Making these assumptions means that some 3-dimensional processes are not modeled in the programs, or are not modeled in a correct way. In this thesis only the shallow water equations are used, since 3Di cannot model 3-dimensional. This chapter describes the derivation from the Navier-Stokes equations to the shallow water equations together with all the used assumptions. For an extensive explanation reference is made to Vreugdenhil (1994), Chapter 2. The first three sections in this thesis are a summary of Chapter 2 Vreugdenhil (1994).

3.1 Reynolds averaged Navier-Stokes equations

The scale of motion has a wide range when working in flows like rivers. Solving all fluctuations on these scales is impossible, since it would require enormous computational force. Usually, the interest is only in the large-scale features. Hence, the small-scale features should be isolated in order to solve the other characteristics. This can be done by decomposing the velocity vector and pressure into a mean value and a fluctuating value.

$$u = \bar{u} + u' \tag{3.1}$$

Since there is no information yet whether the flow is stationary or time-dependent, the mean value can be best determined by ensemble averaging instead of time-averaging (Uijttewaal, 2015). If the flow is stationary both averaging processes are equal to each other if the averaging period is long.

The decomposition is substituted into the Navier-Stokes equation followed by averaging. The result is the Reynolds averaged Navier-Stokes equations (RANS). Appendix B gives a full derivation of these equations.

$$\frac{\partial \rho\bar{u}}{\partial t} + \nabla \cdot (\rho\bar{u}\bar{\mathbf{v}}) + \nabla \cdot \left(\rho\overline{u'\mathbf{v}'}\right) = -\frac{\partial \bar{p}}{\partial x} + \rho f\bar{v} + \nabla \cdot (2\mu\nabla^s\bar{u}) + \bar{F}_x \tag{3.2}$$

$$\frac{\partial \rho\bar{v}}{\partial t} + \nabla \cdot \left(\rho\bar{v}\bar{\mathbf{v}'}\right) + \nabla \cdot \left(\rho\overline{v'\mathbf{v}}\right) = -\frac{\partial \bar{p}}{\partial y} - \rho f\bar{u} + \nabla \cdot (2\mu\nabla^s\bar{v}) + \bar{F}_y \tag{3.3}$$

$$\frac{\partial \rho\bar{w}}{\partial t} + \nabla \cdot \left(\rho\bar{w}\bar{\mathbf{v}'}\right) + \nabla \cdot \left(\rho\overline{w'\mathbf{v}}\right) = -\frac{\partial \bar{p}}{\partial z} - \rho g + \nabla \cdot (2\mu\nabla^s\bar{w}) \tag{3.4}$$

where $\nabla^s = \frac{1}{2}\nabla(\cdot) + \frac{1}{2}\nabla(\cdot)^T$, the symmetric operator, and F_i other driving forces that might occur. These equations look like the Navier-Stokes equations except for one extra term in each of the equations. These terms can be seen as stresses, called the Reynold stresses, and represent the exchange of momentum by turbulent motion.

In the next sections the bar over the variables will be omitted in the equations. However, it should be noted that it is still about the Reynolds averaged quantities.

3.2 Boundary conditions

Solving a partial differential equation means one needs boundary conditions. These conditions are applied at the boundary of a domain of interest. In a river boundary conditions are needed at the bottom, surface and both upstream and downstream of the area of interest. The latter are not treated here, since these boundaries are not defined yet. The conditions at the bottom and surface can be divided into kinematic and dynamic boundary conditions. The first state that no water particle can pass the boundary, while the second are related with the force balance.

- Kinematic boundary condition at solid bottom:

$$u\frac{\partial z_b}{\partial x} + v\frac{\partial z_b}{\partial y} - w = 0 \qquad \text{at } z = z_b \tag{3.5}$$

  where $z_b = \zeta - h$ the bottom level above reference level, and ζ the water level above reference level (Figure 2.1).

- Kinematic boundary condition at free water surface:

$$\frac{\partial \zeta}{\partial t} + u\frac{\partial \zeta}{\partial x} + v\frac{\partial \zeta}{\partial y} - w = 0 \qquad \text{at } z = \zeta \tag{3.6}$$

- Dynamic boundary condition at solid bottom:

$$u = v = 0 \qquad \text{at } z = z_b \tag{3.7}$$

  the "no-slip" condition. It can be seen as viscous fluid that sticks to the boundary, in this case the bottom (Vreugdenhil, 1994).

- Dynamic boundary condition at free water surface:

$$p = p_a \qquad \text{at } z = \zeta, \tag{3.8}$$

  where p_a is the atmospheric pressure.

3.3 Scaling

To go from the RANS equations to the shallow water equations it is assumed that any vertical scale H is much smaller than the horizontal scales L. This results into a flow that can be seen as a boundary-layer form. Using dimensionless numbers the vertical momentum equation can be written in its non-dimensional form. The advantage of this technique is that it is easy to find the order of magnitude of each term. Hence, determining which terms can be neglected and which are important.

Let the terms x and y be of order L and z of the order H, whereas the velocities u and v are of order U. The continuity equation gives that the scale of the vertical velocity w should be of the order UH/L. Using these scales in the vertical momentum equation results into the following ratios:

$$\begin{aligned} \text{local acceleration} \quad & \frac{FrH^2}{L^2} \\ \text{advective terms} \quad & \frac{Fr^2H^2}{L^2} \\ \text{stress gradients} \quad & \frac{Fr^2H}{ReL} \end{aligned} \tag{3.9}$$

where Fr is the Froude number and Re the Reynolds number.

$$Fr = \frac{U}{\sqrt{gH}}, \qquad Re = \frac{UH}{\nu} \tag{3.10}$$

In rivers the Reynolds number can have orders of 10^5, while the Froude number usually has a small order, 10^{-1}. Using these values in the above ratios these will be relative small compared to the gravitational term. This results in two remaining terms, the pressure gradient and the gravitational acceleration.

$$\frac{\partial p}{\partial z} = -\rho g \tag{3.11}$$

This balance is known as the hydrostatic pressure distribution. Integration over the waterdepth results in an expression for the pressure. This expression is only valid if the density assumed constant over the depth, otherwise the pressure gradient will depend on z.

$$p = \rho g(\zeta - z) + p_a \tag{3.12}$$

with p_a the atmospheric pressure. Substitution into the momentum equations leads to

$$\frac{\partial u}{\partial t}+\frac{\partial u^2}{\partial x}+\frac{\partial uv}{\partial y}+\frac{\partial uw}{\partial z}-fv+g\frac{\partial \zeta}{\partial x}+\frac{g}{\rho_0}(\eta-z)\frac{\partial \rho}{\partial x}+\frac{1}{\rho_0}\frac{\partial p_a}{\partial x}-\frac{1}{\rho_0}\left(\frac{\partial \tau_{xx}}{\partial x}+\frac{\partial \tau_{yx}}{\partial y}+\frac{\partial \tau_{zx}}{\partial z}\right)=0$$
$$\frac{\partial v}{\partial t}+\frac{\partial uv}{\partial x}+\frac{\partial v^2}{\partial y}+\frac{\partial vw}{\partial z}+fu+g\frac{\partial \zeta}{\partial y}+\frac{g}{\rho_0}(\eta-z)\frac{\partial \rho}{\partial y}+\frac{1}{\rho_0}\frac{\partial p_a}{\partial y}-\frac{1}{\rho_0}\left(\frac{\partial \tau_{xy}}{\partial x}+\frac{\partial \tau_{yy}}{\partial y}+\frac{\partial \tau_{zy}}{\partial z}\right)=0 \tag{3.13}$$

where ρ_0 is the reference density.

3.4 2D shallow-water equations

The final step is to integrate Equations (3.13) and the continuity equation over the depth $h=\zeta-z_b$. The depth averaged values are defined as:

$$\bar{u}=\frac{1}{h}\int_{z_b}^{\zeta}u dz. \tag{3.14}$$

Integration of the continuity equation is given as an example. The other integrations are fully described in Appendix B.

$$\begin{aligned}\int_{z_b}^{\zeta}\frac{\partial u}{\partial x}+\frac{\partial v}{\partial y}+\frac{\partial w}{\partial z}dz =&\frac{\partial}{\partial x}\int_{z_b}^{\zeta}u dz-u^s\frac{\partial \zeta}{\partial x}+u^b\frac{\partial z_b}{\partial x}+\frac{\partial}{\partial y}\int_{z_b}^{\zeta}v dz-..\\ &..-v^s\frac{\partial \zeta}{\partial y}+v^b\frac{\partial z_b}{\partial y}+w^s-w^b\\ =&\frac{\partial \zeta}{\partial t}+\frac{\partial h\bar{u}}{\partial x}+\frac{\partial h\bar{v}}{\partial y}=0\end{aligned} \tag{3.15}$$

where the Leibniz Integral Rule is used at the first line and boundary conditions (3.5) and (3.6) at the second line. s and b stand respectively for surface and bottom in the above equation. Using similar operations for the momentum equations and omitting the overbar, the resulting shallow water equations are

$$\frac{\partial hu}{\partial t}+\frac{\partial hu^2}{\partial x}+\frac{\partial huv}{\partial y}-fhv+gh\frac{\partial h}{\partial x}+\frac{gh^2}{2\rho_0}\frac{\partial \rho}{\partial x}-\frac{1}{\rho_0}\tau_{bx}-\frac{\partial}{\partial x}\left(hT_{xx}\right)-\frac{\partial}{\partial y}\left(hT_{xy}\right)=F_x$$
$$\frac{\partial hv}{\partial t}+\frac{\partial huv}{\partial x}+\frac{\partial hv^2}{\partial y}+fhu+gh\frac{\partial h}{\partial y}+\frac{gh^2}{2\rho_0}\frac{\partial \rho}{\partial y}-\frac{1}{\rho_0}\tau_{by}-\frac{\partial}{\partial x}\left(hT_{yx}\right)-\frac{\partial}{\partial y}\left(hT_{yy}\right)=F_y \tag{3.16}$$

with $F_{x,y}$ the driving forces including wind, radiation stresses, and the atmospheric pressure gradient and T_{ij} the lateral stresses that include viscous friction, turbulent friction and differential advection (Vreugdenhil, 1994):

$$T_{ij}=\frac{1}{h}\int_{z_b}^{\zeta}\left(\nu\left(\frac{\partial u_i}{\partial x_j}+\frac{\partial u_j}{\partial x_i}\right)-\overline{u_i'u_j'}+(u_i-\overline{u_i})(u_j-\overline{u_j})\right)dz \tag{3.17}$$

These equations are usually not the "standard" form of the shallow water equations. The "standard" form is obtained by neglecting some of the processes and assuming a few parameterizations. However, these are not explained here but in the next section together with the equations used in FM and 3Di.

3.5 Assumptions

The shallow water equations that are used in FM and 3Di are different from the one that were derived above, except for the conservation of mass. The differences between both momentum equations, together with an explanation of new terms, are described after the next equations. Conservation of momentum for both programs is as follows ((Deltares, 2015), (Stelling, 2012)),

$$\text{3Di } x-\text{direction} \quad \frac{\partial u}{\partial t}+u\frac{\partial u}{\partial x}+v\frac{\partial u}{\partial y}+g\frac{\partial \zeta}{\partial x}+\frac{c_f}{h}u\|u\|=0 \tag{3.18}$$

$$y-\text{direction} \quad \frac{\partial v}{\partial t}+u\frac{\partial v}{\partial x}+v\frac{\partial v}{\partial y}+g\frac{\partial \zeta}{\partial y}+\frac{c_f}{h}v\|u\|=0 \tag{3.19}$$

$$\text{FM } x-\text{direction} \quad \frac{\partial u}{\partial t}+u\frac{\partial u}{\partial x}+v\frac{\partial u}{\partial y}+g\frac{\partial \zeta}{\partial x}+\frac{c_f}{h}u\|u\|=\frac{1}{h}\nabla\cdot\left(\nu h\left(\nabla u+\nabla u^T\right)\right) \tag{3.20}$$

$$y-\text{direction} \quad \frac{\partial v}{\partial t}+u\frac{\partial v}{\partial x}+v\frac{\partial v}{\partial y}+g\frac{\partial \zeta}{\partial y}+\frac{c_f}{h}v\|u\|=\frac{1}{h}\nabla\cdot\left(\nu h\left(\nabla v+\nabla v^T\right)\right) \tag{3.21}$$

which is the non-conservative form of the shallow water equations, whereas the equations in Section 3.4 are in conservative form. It can be seen when Equation (3.16) and the above are compared many terms are missing or different. Hence, there are some processes that are neglected and some that are simplified. Below these are described together with assumptions that were needed to go from the Navier-Stokes equations to the 2D shallow water equations (Vreugdenhil, 1994).

Boundary layer form

A boundary layer form is assumed. Hence, all terms except the pressure gradient in the vertical momentum equations are small relative to the gravitational acceleration. This results in a pressure that is hydrostatic distributed and the simplified terms $\left(g\frac{\partial \zeta}{\partial x}, g\frac{\partial \zeta}{\partial y}\right)$ instead of $\left(\frac{\partial p}{\partial x}, \frac{\partial p}{\partial y}\right)$. Looking at a river one can assume that the acceleration and eddy viscosity terms are much smaller than the gravitational acceleration. However, when there are structures in a river, like groynes, these terms cannot always be neglected. Consequences are that the velocity is underestimated, since acceleration in the vertical direction is neglected.

Driving forces

Driving forces (F_x, F_y) are neglected:

- The atmospheric pressure gradient $\left(\frac{\partial p_a}{\partial x}, \frac{\partial p_a}{\partial y}\right)$ can be important when a storm surge is simulated. Looking only at rivers it can be neglected.
- Wind stresses are not present in the shallow water equations. In both programs there is however the possibility to turn it on.
- It was assumed that the density is constant in the vertical direction, since the depth-averaged equations are used. This led to a linear relation between pressure and density (Equation (3.12)). When there is no stratification, or it is negligible, this will be no problem. Otherwise, a 2DH model will not suffice anymore. This does not mean that the density is constant in the horizontal plane. These density gradient s$\left(\frac{\partial \rho}{\partial x}, \frac{\partial \rho}{\partial y}\right)$, present in Equation (3.16), usually have a small influence compared with other terms and are therefor often neglected.
- Radiation and tidal stress are of less importance in modeling rivers than in coastal areas or oceans. Neglecting these terms will therefor not have a large impact.

Coriolis force

The Coriolis effect in Equation (3.16) is left out. Whether this assumption is acceptable can be seen with the Rossby number, Ro$= U/fL$. It represents the ratio between inertia and Coriolis terms. When it is of the order 1 or higher, the Coriolis effect can be neglected, since it is of minor importance. In the case of rivers, the length scale is of the order of $10^3 - 10^4$ m and the velocity of order 1 m/s. Looking at rivers in countries like the Netherlands or Germany gives a Coriolis parameter of order 10^4. Using these values gives a Rossby number of the order 1. Hence, the assumption of neglecting the Coriolis force is acceptable.

Bottom stress

The bottom stress is expressed as $\tau_{bx}/\rho = c_f u\|u\|$, where $\|\cdot\|$ is the L2-norm. Hence, $\|u\| = \sqrt{u^2 + v^2}$. This parameterized form is needed to have a closed system of equations. It originates from the similarities with the equilibrium between turbulent boundary layers. Thus, if the fluid has a analogous flow this supposition is assumed correct. The coefficient c_f is a standard friction coefficient which depends on the wall roughness. It can for example be approximated by Chezy, or Manning.

Lateral stresses

Lateral stresses T_{ij} where $i, j = x, y$:

- The viscous stresses are neglected. In realistic situations the order of magnitude is small compared to the other therms, hence, consequences of neglecting the viscous stresses will be small.
- A river bend has a secondary flow that results from centrifugal and pressure forces in the intersection. Looking at a cross section of the river in a bend, see Figure 3.1, it can be seen that in the upper part the flow is directed towards the outer bend and in the lower part towards the inner bend. When the bend is only mildly curved the amount of water flowing outwards is almost equal to the inwards water flow. Usually the main velocity has a profile that is more or less a logarithmic

distribution. Hence, the mean velocity is higher at the upper part than the lower part. Combining the secondary flow and the main velocity results in a helical flow, Figure 3.2. It can be seen that there is more momentum transported to the outer

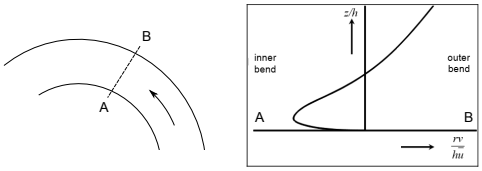

Figure 3.1: Secondary flow in a bend

part of the bend than the inner part. It results in a higher velocity at the outer part of the bend which is at the cost of the flow velocity at the inner bend. This is known as differential advection (Jirka and Uijttewaal, 2004). If it is not taken into account it would mean that the flow velocity at the outer bend is underestimated, while the velocity at the inner bend is overestimated.

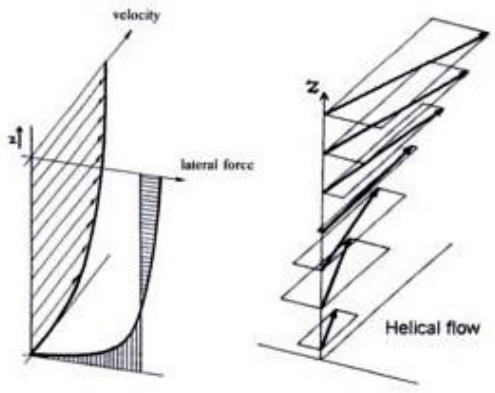

Figure 3.2: Helical flow (Jirka and Uijttewaal, 2004)

- One of the processes that is neglected in 3Di but not in Flexible Mesh is the diffusivity. Consequences are that turbulent processes are not modeled in 3Di. In Civil Engineering applications almost all flows are turbulent, including river flows. If only information about the mean flow is needed the absence of turbulence is of less importance compared to information needed about velocity profiles behind groynes. In FM turbulent shear stress is approximated similar to viscous shear stress. This results in one missing expression for the turbulent viscosity. Flexible Mesh uses Elder to estimate the horizontal turbulence viscosity.

3.6 Difference in processes in 3Di and Flexible Mesh

At this moment the possibilities in Flexible Mesh are greater than in 3Di. Of course, it is important to know both differences and similarities. In this section the processes of interest are shortly described.

Friction

Flexible Mesh and 3Di have different options to model bottom friction. In the previous section it was already seen that the bottom stress is expressed as $\tau = \rho c_f u \|u\|$, with c_f a standard friction coefficient. This coefficient can be determined with the following formulations.

Chezy:

$$u = C\sqrt{Ri} \tag{3.22}$$

where C is the Chezy coefficient, R the hydraulic radius en i the bed slope. It can be related to c_f by $C = \sqrt{g/c_f}$. This formulation originates from the fact that there is a balance between the force driving flow and the total friction force and that the latter is a function of a roughness coefficient and the velocity squared.

Manning:

$$u = \frac{1}{n} R^{2/3} \sqrt{i} \tag{3.23}$$

with n the Manning coefficient. This coefficient has the following relation with the Chezy coefficient, $C = R^{1/6}/n$. Manning's formulation is most commonly used in open channel flows

White-Colebrook:

$$\frac{1}{\sqrt{c_f}} = -2 \log \left(\frac{\epsilon}{14.8R} + \frac{2.51}{Re\sqrt{c_f}} \right) \tag{3.24}$$

a formula that calculates directly the friction coefficient with ϵ the roughness height. It is only present in Flexible Mesh and not in 3Di. Above a relation with the Chezy coefficient was already given. Looking at this formula it is seen that there is a log function. Thus, a logarithmic velocity profile is assumed in the vertical direction. Of course, when using the depth-averaged equations this profile is spread over the depth. However, it is physically not correct anymore to use these formulas. Using 2-dimensional models instead of 3-dimensional implies implicitly that the flow is fully developed. When modeling rivers it should be kept in mind whether these formulas are physically correct when used.

Diffusivity

This term is neglected in 3Di as seen before. In Flexible Mesh it is calculated by the term

$$\nabla \cdot \left(\nu h(\nabla u + \nabla u^T)\right). \tag{3.25}$$

In Section 3.1 the Reynolds-averaged Navier-Stokes equations were derived. The $x-$direction is taken as an example to see where this diffusion term arises from. There are two terms in Equation (3.2) that represent stresses,

$$\nabla \cdot (\overline{\rho u' v'}), \text{ and } \qquad \nabla \cdot (2\mu \nabla^s \bar{u}). \tag{3.26}$$

Remember that the overline in this case represents the time-averaged. These terms can be taken together. Then,

$$\begin{aligned} \frac{\partial}{\partial x}\tau_{xx} &= \frac{\partial}{\partial x}\left(\rho\overline{u'u'} + 2\mu\frac{\partial u}{\partial x}\right) \\ \frac{\partial}{\partial y}\tau_{xy} &= \frac{\partial}{\partial y}\left(\rho\overline{u'v'} + \mu\left(\frac{\partial u}{\partial y} + \frac{\partial v}{\partial x}\right)\right) \end{aligned} \tag{3.27}$$

In order to close the equation system, the turbulent shear stress needs to be approximated by a relation proportional with the mean velocity field. This is done as follows,

$$\begin{aligned} \tau_{t,xx} &= \rho\overline{u'u'} = -2\rho\nu_t\frac{\partial u}{\partial x}, \\ \tau_{t,xy} &= \rho\overline{u'v'} = -\rho\nu_t\left(\frac{\partial u}{\partial y} + \frac{\partial v}{\partial x}\right) \end{aligned} \tag{3.28}$$

where ν_t is the turbulent viscosity, or eddy viscosity. When there is a high Reynolds number, the flow is highly turbulent. This implies that the molecular viscosity shear stresses are much smaller than the turbulent shear stresses. For flows near a wall this is not true. Hence, they can be neglected, giving

$$\begin{aligned} \frac{\partial}{\partial x}\tau_{xx} &= \frac{\partial}{\partial x}\left(-2\rho\nu_t\frac{\partial u}{\partial x}\right) \\ \frac{\partial}{\partial y}\tau_{xy} &= \frac{\partial}{\partial y}\left(-\rho\nu_t\left(\frac{\partial u}{\partial y} + \frac{\partial v}{\partial x}\right)\right). \end{aligned} \tag{3.29}$$

Or, generally written in the shallow water equations,

$$\nabla \cdot \left(\nu h(\nabla u + \nabla u^T)\right). \tag{3.30}$$

Notice that the kinematic viscosity is thus the turbulent viscosity, and not the molecular viscosity which is much smaller in turbulence flows.

Grid

Grid differences were shortly mentioned in Chapter 2. Chapter 4 en 5 will continue with describing this grid generation of both programs. It will not be treated here.

The goal with these differences and similarities is to first make models that are as similar as possible in order to compare them in the same situation. The grid will, however, not be the same since this is what both tools make unique. Possible differences in both programs can then hopefully be reduced to grid generation. It is clear that Flexible Mesh has more options in the modeling. The second step will be to use other processes to run models and compare them with the results where both models were made as similar as possible.

Chapter 4

D-Flow Flexible Mesh

One of the main differences between Flexible Mesh and 3Di is the way a grid is generated. Whereas 3Di generates a Cartesian grid, Flexible Mesh uses a combination of an unstructured and structured grid. The latter can consist of a curvilinear or rectangular grid. This combination makes it possible to model numerically complex geometries in a more precise way. When equations are discretised Flexible Mesh has several options to choose from. It will be made clear when this appears together with an explanation of the choice made. This chapter will explain the grid generation of Flexible Mesh, together with the discretisation of the shallow water equations. The main part of this chapter is from the Technical Reference of Delft3D D-Flow Flexible Mesh (Deltares, 2015).

4.1 Grid generation

Before the discretisation of the shallow water equations is done, an introduction of some notations and properties that are important for this discretisation is given. Flexible Mesh works both with a structured and unstructured grid. Generating such a grid can be very complicated compared to a Cartesian grid. There are two important properties that have to be taken into account. These are orthogonality and smoothness. The orthogonality is measured by taking the cosinus of the angle between the netlink and flowlink. See Figure 4.1 for the definitions of these terms. Smoothness is defined by the ratio of two adjacent cell areas. In a perfect grid generation both of these parameters would be equal to one. Hence, the netlink has an angle of 90° with the flowlink. An example of both parameters that are ideal is given in Figure 4.2. It can be seen that the flowlink is a line between two flownodes. Flownodes are the centers of a cell, that can be defined in different ways. These are explained later in this chapter.

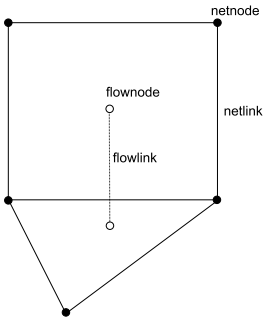

Figure 4.1: Net (domain discretisation)

The discretisation is done with a staggered grid, hence, water levels are calculated at the cell center while velocities are calculated at the cell faces' midpoints. For a rectangle the cell center is easy to see. However, looking at a triangle there are multiple ways to define a cell center.

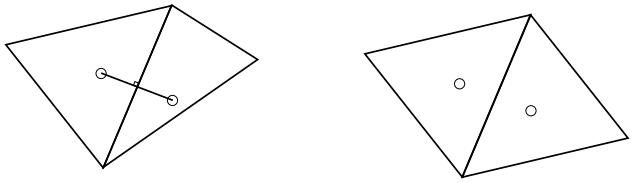

Figure 4.2: Perfect orthogonality (left) and perfect smoothness (right)

One of them is the center of a circle that intersects the triangle at each node. The other possibility is the gravity point of the triangle itself, the mass center. Flexible Mesh uses the first possibility, since with this option the orthogonality property is easier to fulfil. One of the disadvantages of using a circumcenter is that the center can lie outside the triangle. When Flexible Mesh construct a grid automatically this usually will not happen. Otherwise, there are many options that can be performed, like changing the minimal and maximal angle of a triangle. In this way triangles with an outlying circumcenter are easier to avoid. Another disadvantage is that the flow link can approach zero. Hence, the flownodes of two adjacent cells are too close together, see Figure 4.3a. It shows that the white dots, cell centers, inside the red circle are almost on top of each other. The flow link that connects both cell centers will be very small, which leads to high errors. This can be solved by removing that certain flowlink as seen in Figure 4.3b. Notice that the two white dots are not connected with each other.

Removing a flowlink, as is done in Figure 4.3b, has consequences for the flow and the grid. The common face between these two cells is removed from the grid. Instead, an invisible, infinite high wall arises where no water can go through. Figure 4.4 shows what happens. If the flowlink was not removed, the velocity vectors would be only directed in the $x-$direction, since there are no obstacles. Now, one can see that the flow is going around something invisible. If this happens, the velocity profile resulting from a model is physically not correct. This is why the cell centers should be inside the triangles and not too close to their edges.

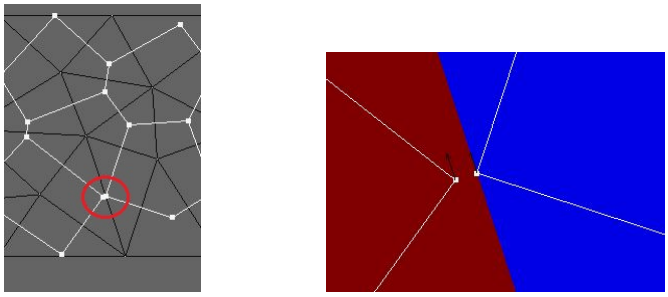

(a) Grid with flowlinks

(b) Removed flowlink

Figure 4.3: Small flowlinks

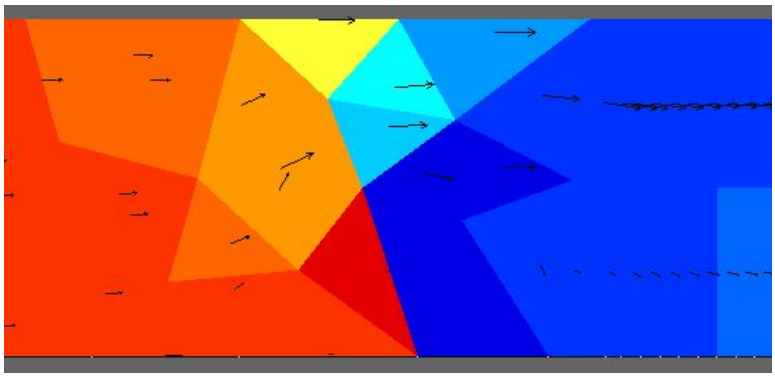

Figure 4.4: Behaviour of the flow when a flowlink misses

4.1.1 Connectivity

In this subsection a few important expressions are introduced. These are needed in order to understand the following part of the report. Figure 2.2 showed a 3-dimensional cell together with some definitions. The cells in Flexible Mesh can take multiple forms, like rectangular, curvilinear, and triangular prism but also a prism with more than four nodes on top and bottom base. The most common shape in Flexible Mesh are the first three. Since it is easy to extend the following definitions to a rectangular prism, only the triangular prism is taken as an example, also in the remainder of this chapter.

All vertical faces j of a cell k are contained in a set $\mathcal{J}(k)$. The mesh nodes i of a cell k are in a set $\mathcal{I}(k)$. Each face j has mesh nodes $i_{L(j)}, i_{R(j)}$. It depends on the orientation of face j which node belongs to $i_{L(j)}$ or $i_{R(j)}$. The same applies to the neighbour cells $L(j), R(j)$ for face j. This orientation can be taken into account by $1_{j,k}$, which is

$$1_{j,k} = \begin{cases} 1, & L(j) = k \quad (\mathbf{n}_j \text{ is outward normal of cell k}) \\ -1, & R(j) = k \quad (\mathbf{n}_j \text{ is inward normal of cell k}). \end{cases} \tag{4.1}$$

$\mathbf{n}_f$ is the normal vector of face j (Deltares, 2015). If we take two cells as in Figure 4.5, then $\mathcal{J}(1) = \{1, 2, 3\}$ and $\mathcal{J}(2) = \{4, 5, 1\}$. The set of mesh nodes is given by $\mathcal{I}(1) = \{1, 2, 3\}$ for cell $k = 1$ and $\mathcal{I}(2) = \{1, 2, 4\}$ for cell $k = 2$. For face 1 an outward normal vector is found for cell $k = 1$. Hence, $L(1) = 1$, $R(1) = 2$ and $i_L(1) = 2$, $i_R(1) = 1$.

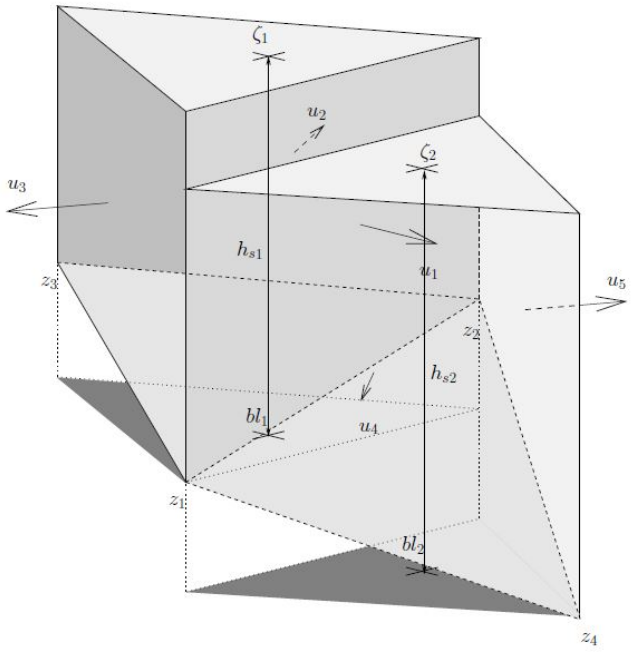

Figure 4.5: Example of notations (Deltares, 2015)

4.1.2 Bed geometry

In Flexible Mesh there are multiple options to define the bed geometry. In Section 4.1.1 the cell-based bed level was already shown in Figure 4.5. Its value depends on the type of bed level one chooses. For all available options one can go to the Technical Reference of Deltares (2015). In this thesis bed level type 3 is chosen in combination with a conveyance type ≥ 1, explained below. This results in the possibility to model the bottom linearly. Usually a uniform bed representation is used. However, a linearly representation gives a more accurate description of the total wet cross sectional area.

$$\begin{aligned} bob_{1,2_j} &= z_{i_{L,R}(j)} \\ bl_k &= \min_{j \in \mathcal{J}(k)} [\min(bob_{1j}, bob_{2,j})] \end{aligned} \tag{4.2}$$

with $bob_{1,2_j}$ the face-based bed-levels and z_i the node-based bed levels. Choosing bed-level type 3 in combination with conveyance ≥ 1 gives that the face- and node-based bed levels are the same. The type of conveyance gives how the friction is defined. When a bottom is linearly modelled in a cell, the water depth is a function inside this cell. This also means that the velocity is not constant, hence, the bed stresses differ inside this cell. If a closer look is taken at the friction term,

$$\text{friction} = \frac{gu\|u\|}{C^2\hat{h}} \tag{4.3}$$

with $\hat{h}$ the hydraulic radius. It can be seen that it depends both on the normal and tangential velocity. Both are variable for the width of a cell. For the conveyance there are 3 types that are possible that are ≥ 1:

Type of conveyance	Normal velocity	Tangential velocity	Water depth	Friction coefficient	Note
1	$u(y)$	$v(y)$	$\hat{h}(y)$	C	All terms are linear varying over the width.
2	$u(y)$	zero	$\hat{h}(y)$	C	Only applicable for a curvilinear grid aligned with the flow.
3	constant	constant	$h = A/P$	C	With a sufficient resolution of a gully in the grid just as good as 1 and 2. However, computational time is 10% faster.

A is the wet cross sectional area and P the wet perimeter.

With the type of bed level known, the wet cross-sectional can be calculated as well. This is the area of a cell face that is wet. When looking at this area there are two possibilities. The first is that the cell face is entirely wet (Figure 4.6), while the second is that it is only partly wet.

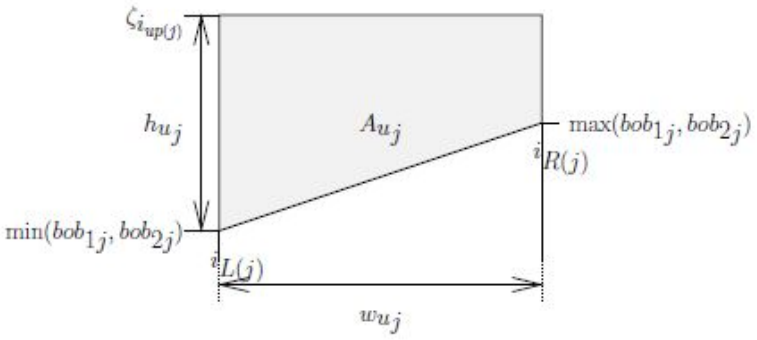

Figure 4.6: Flow area A_{uj} and face-based water depth h_{uj} (Deltares, 2015)

Let $\Delta b_j = \max(bob_{1j}, bob_{2j}) - \min(bob_{1j}, bob_{2j})$, and

$$h_{uj} = \begin{cases} \zeta_{L(j)} - \min(bob_{1j}, bob_{2j}), & u_j > 0 \quad \text{or} \quad u_j = 0 \text{ and } \zeta_{L(j)} > \zeta_{R(j)} \\ \zeta_{R(j)} - \min(bob_{1j}, bob_{2j}), & u_j < 0 \quad \text{or} \quad u_j = 0 \text{ and } \zeta_{L(j)} \leq \zeta_{R(j)} \end{cases} \tag{4.4}$$

where the water level $\zeta_{L,R}$ is obtained by first order upwinding. Hence, there is an error

of second order. This is one of the main disadvantages of using unstructured grids. They usually do not have a high-order accuracy (Perot, 2000). Using these expressions the wet cross-sectional can be defined as

$$A_{uj} = \begin{cases} w_{uj} h_{uj}, & \Delta b_j < 10^{-3} w_{uj} \\ w_{uj} h_{uj} \min(\frac{h_{uj}}{\Delta b_j}, 1) \left(1 - \frac{1}{2} \min(\frac{\Delta b_j}{h_{uj}}, 1)\right), & \text{otherwise} \end{cases} \tag{4.5}$$

with w_{uj} the width. When $\frac{h_{uj}}{\Delta b_j} < 1$ one obtains the rule of calculating areas of triangles. If $\frac{\Delta b_j}{h_{uj}} < 1$ it is a rule for a trapezium.

4.2 Discretisation of shallow water equations

In Section 3.5 the shallow water equations were given like they are implemented in Flexible Mesh. The following subsections contain the spatial and temporal discretisation of these equations.

4.2.1 Spatial discretisation

For cell k the following continuity equation is found,

$$(V_k)_t + \sum_{j \in \mathcal{J}(k)} A_{uj} u_j 1_{j,k} = 0 \tag{4.6}$$

where, as said before, $1_{j,k}$ takes into account the orientation of face j with respect to cell k, and A_{uj} is the wet cross-sectional area. Since the finite volume method is used to discretize the continuity equation it is guaranteed that there is mass conservation. This can be easily seen in the discretized continuity equation. At each cell face there is an incoming or outgoing flux (depended on the value of $1_{1,k}$). At the neighbouring cell this is exactly the opposite sign. Hence, the mass fluxes cancel each other inside the domain channel (Borsboom, 2013). Thus, leaving only the fluxes at the boundary.

Discretisation of the momentum equations is a bit harder than the continuity equation, since it takes place at the faces of a cell.

$$(u_j)_t + \mathcal{A}_{ij} u_j + \mathcal{A}_{ej} + \frac{g}{\Delta x_j} \left(\zeta_{R(j)} - \zeta_{L(j)}\right) + \frac{g \|u_j\|}{C^2 \hat{h}} u_j = 0 \tag{4.7}$$

with $\hat{h}$ the hydraulic radius. The second and third terms are the discretized advection and diffusion term, where $\mathcal{A}_{ij}$ denotes the implicit terms and $\mathcal{A}_{ej}$ explicit terms. They will be better explained below. The fourth term is the water level gradient. By assuming an orthogonal grid the water level gradient can be determined by central differencing, which results in a second order local error.

$$g \nabla \zeta|_j \cdot \mathbf{n}_j \approx \frac{g}{\Delta x_j} (\zeta_{R(j)} - \zeta_{L(j)}) + \mathcal{O}(\Delta x_j^2) \tag{4.8}$$

where Δx_j is the distance between the two circumcenter points where the water levels are defined. It has been observed in Chapter 3 that the bottom friction is an unknown variable which has to be expressed in the mean velocity field and a friction coefficient. Section 3.6 gave the possibilities to determine this friction coefficient. Notice that in Equation (4.7) the Chezy formulation is used.

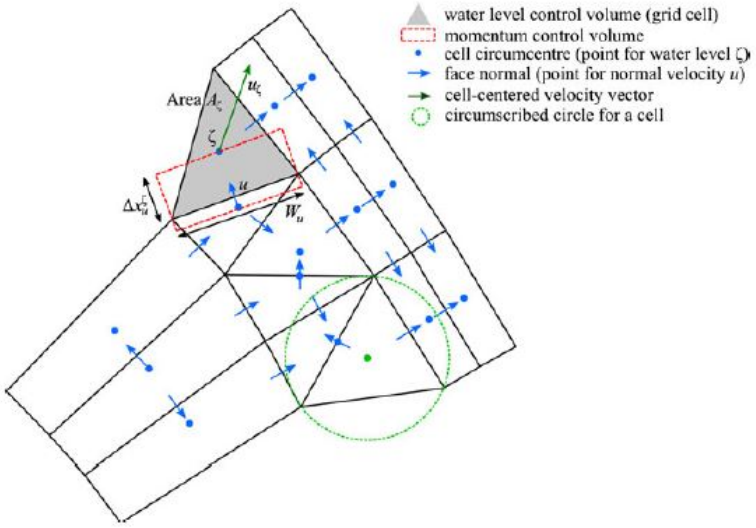

Figure 4.7: Control volumes of triangular grid (Kernkamp et al., 2011)

Whereas for mass there is both local and global conservation, this cannot be said for momentum. Only global conservation of momentum can be proven (Borsboom, 2013). This is the result of the control volumes of momentum. Figure 4.7 shows among other things the momentum control volume for a face-normal velocity. It can be seen that it is a rectangle which has in one direction the length between common grid points and in the other direction a length of the distance between the circumcenters of both cells. If in this way the momentum control volume for another adjacent cell of the triangular cell is taken, one would see that they overlap. In order to prove local momentum conservation it is needed to discretize the momentum equation for non-overlapping control volumes, which is not possible for arbitrary triangular cells (or even all quadrilateral grid cells). When there is a rectangular grid, the control volumes will not overlap and there will be local momentum conservation.

Momentum advection

The momentum equations are solved in the face-normal directions, hence, not the complete momentum vector is solved. It was said before that momentum conservation is locally not conservative. Flexible Mesh is not able to define conservative fluxes, since only the face-normal velocity is solved. Following the method of Perot (2000), who achieved momentum conservation for unstructured staggered mesh schemes, multiple advection schemes are thought of. However, none of these schemes is conservative as the method of Perot (2000). The idea behind Perot's method is to reconstruct face-normal velocities to cell-centered velocities. Here a discretisation is performed, whereafter these velocities

are interpolated back to the faces. The final step is to project these velocities in the face-normal direction. This thesis will not elaborate further on the method of Perot (2000). A more detailed idea is given in Deltares (2015). The advection term as implemented in FM is given by

$$\begin{aligned}\mathcal{A}_{ej} =& \frac{\alpha_j}{\alpha_j V_{L(j)} + (1-\alpha_j)V_{R(j)}} \sum_{l \in \mathcal{J}(L(j))} q_{al} 1_{l,L(j)} \mathbf{u}_{ul} \cdot \mathbf{n}_j - q_{al} 1_{l,L(j)} u_j + .. \\ .. &+ \frac{1-\alpha_j}{\alpha_j V_{L(j)} + (1-\alpha_j)V_{R(j)}} \sum_{l \in \mathcal{J}(R(j))} q_{al} 1_{l,R(j)} \mathbf{u}_{ul} \cdot \mathbf{n}_j - q_{al} 1_{l,R(j)} u_j \\ \mathcal{A}_{ij} =& 0,\end{aligned} \tag{4.9}$$

where $\mathbf{u}_{ul}$ is the reconstructed full velocity at the faces obtained by upwinding the cell-centered velocities. The discrete cell-centered approximation is first-order accurate unless the mass and center point (here circumcenter) are close together. In this case it is a second order approximation. Further, q_{al} fluxes, u_j the face-normal velocity and α_j the non-dimensional distance from the left cell center to the face.

Momentum diffusion

Discretisation of diffusion has the same approach as the momentum advection. The term is first discretised at the cell centers whereafter it is interpolated to the faces and then projected in the face normal direction. Section 3.5 showed the diffusion term as it is in the momentum equation. In Flexible Mesh this term is a bit altered,

$$\frac{1}{h^p} \nabla \cdot (\nu h^p (\nabla \mathbf{u} + \nabla \mathbf{u}^T)) \tag{4.10}$$

with

$$p = \begin{cases} 1, & \text{istresstype} = 3 \\ 1, & \text{istresstype} = 3 \\ 0, & \text{otherwise.} \end{cases} \tag{4.11}$$

This gives that if istresstype $\neq 3 \wedge \neq 5$ the momentum diffusion does not depend on the water depth. This is, however, incorrect. In this thesis the value 3 will be used. In this way the diffusion term is still dependent on the depth. Another advantage is that in modelling the viscosity coefficient Elder's formula can be used or a Smagorinsky model, not further explained here.

4.2.2 Time discretisation

Time discretisation of the momentum equation is semi-implicit and is as follows

$$\frac{u_j^{n+1} - u_j^n}{\Delta t} + \mathcal{A}_{ij} u_j^{n+1} + \mathcal{A}_{ej} u_j^n + \frac{g\theta_j}{\Delta x_j}(\zeta_{R(j)}^{n+1} - \zeta_{L(j)}^{n+1}) + \frac{g(1-\theta_j)}{\Delta x_j}(\zeta_{R(j)}^{n} - \zeta_{L(j)}^{n}) + \frac{g\|\hat{u}_j\|}{C^2 h} u_j^{n+1} = 0. \tag{4.12}$$

As determined before $\mathcal{A}_{ij} = 0$ and $\mathcal{A}_{ej}$ consists of momentum advection and diffusion. θ_j is a value between 0 and 1 which determines whether the equation is fully implicit, explicit or semi-implicit. Usually its value is around 0.5.

$$u_j^{n+1} = -f_{u_j}^n(\zeta_{R(j)}^{n+1} - \zeta_{L(j)}^{n+1}) + r_{u_j}^n \tag{4.13}$$

with

$$f_{u_j}^n = \frac{1}{B_u}\frac{g\theta_j}{\Delta x_j}, \qquad B_u = \frac{1}{\Delta t} + \frac{g}{C^2 h}\sqrt{(\hat{u}_j^*)^2 + (v_j^n)^2} \tag{4.14}$$

where $\hat{u}_j^*$ is the face normal velocity that follows from a few iterations by taking $\theta = 0$ and solving the momentum equation for $\hat{u}_j$. Further

$$r_{u_j}^n = \frac{1}{B_u}\left(\frac{u_j^n}{\delta t} - \mathcal{A}_{ej} - \frac{g(1-\theta_j)}{\Delta x_j}(\zeta_{R(j)}^n - \zeta_{L(j)}^n)\right). \tag{4.15}$$

The continuity equation is discretized in time as

$$\frac{V_k^{n+1} - V_k^n}{\Delta t} + \sum_{j\in\mathcal{J}(k)} A_{u_j}^n(\theta_j u_j^{n+1} + (1-\theta_j)u_j^n)1_{j,k} = 0. \tag{4.16}$$

Substituting the momentum equation into this equations yields the following system for the water column volume,

$$\frac{V_k^{n+1} - V_k^n}{\Delta t} + \sum_{j\in\mathcal{J}(k)} A_{u_j}^n\theta_j f_{u_j}^n\zeta_k^{n+1} - \sum_{j\in\mathcal{J}(k)} A_{u_j}^n\theta_j f_{u_j}^n\zeta_{O(k,j)}^{n+1} = -\sum_{j\in\mathcal{J}(k)} A_{u_j}^n(\theta_j r_{u_j}^n + (1-\theta_j)u_j^n)1_{j,k} \tag{4.17}$$

where $O(k,j)$ represents the cell that shares face j with cell k. After the water volume is expressed in terms of water levels (not explained here, for technical details see Deltares (2015)) these equations can be solved by a preconditioned Conjugate Gradient method.

Chapter 5

3Di

In Section 3.5 the shallow water equations as used in 3Di were treated. In order to solve these equations numerically the domain has to be approximated by a grid. The way this grid is generated is new in the world of hydraulic engineering. It consists of a coarse grid that can be locally refined by using a quadtree method (further explained in this chapter). This coarse grid is linked to a sub-grid that is able to solve bottom friction and storage on a grid with a high resolution. This gives that the possible errors in both should be reduced, hence, reproduce a better view of reality. This chapter describes the 3Di grid generation together with a detailed description of all important components. All definitions given in this chapter are from the article of Stelling (2012).

5.1 Quadtrees

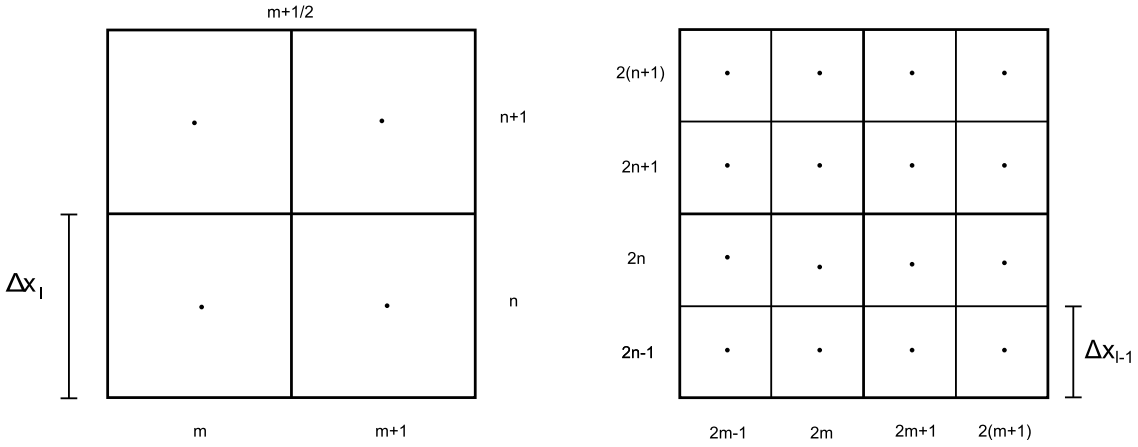

Figure 5.1: Grid cell numbering in two layers

A Cartesian grid is often the most simple grid that can be used for making a numerical model. It has many advantages. One of them is the simplicity. The numerical equations

that are involved are quite simple and the generation of a grid is very easy and quick comparable to other grids. In the past years the disadvantages, see Section 2.2.1, are partly removed by using flow solvers that have the ability to manage with arbitrary and moving boundaries. Adjusting the grid by using quadtrees is a possibility. A quadtree grid distinguishes itself from other grids due to the fact that each square cell can be subdivided into four child cells. Each of these child cells will be of equal size. Hence, a grid using this method can be refined in an easy way. Since multiple methods are combined to create a new method as used in 3Di, the quadtree grid is used a bit different than it is normally used. Using the quadtree method "normal" would mean that the whole domain of interest is placed inside one square, called the root square (Wang et al., 2004). The root square is divided into four child cells and each of the cells is checked to see if it should be divided again. In case of the 3Di grid the root square is the largest grid cell that is used. When there are l layers its grid size is $\Delta x_l \times \Delta y_l$, where $\Delta x_l = \Delta y_l$. Looking at a subdivision level the grid size is $\Delta x_{l-1} \times \Delta y_{l-1}$. Figure 5.1 shows an example of two levels with their grid cell size and the numbering. These are however two different grids. Combining them would look like Figure 5.2. This is how the grid is used in 3Di. It is important that the subdivision level difference between two adjacent cells has a maximum of 1. This results in a balanced quadtree, and only one hanging node (a node on the face between the two cells which does not belong properly to both of the cells) per edge of a cell (Figure 2.5).

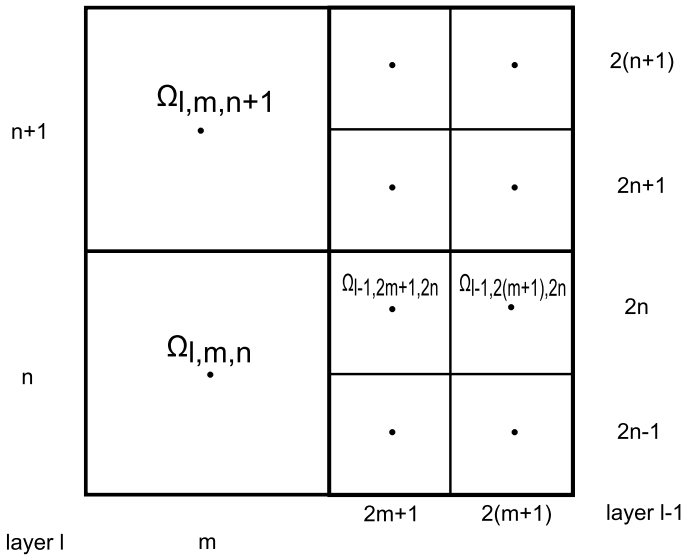

Figure 5.2: Grid cell numbering

5.2 Subgrid

Another change in the flow solver that is used to take out the disadvantages of the Cartesian grid is using a digital element model (DEM), which is a second grid with a different resolution. In this way it is possible to use detailed bathymetry data on a fine Cartesian grid. This fine grid contains the bottom values, while the coarse grid holds the water levels and velocities. Figure 5.3 shows a coarse cell $\Omega_{l,m,n}$ with a sub-grid that

consist of pixels $P_{i,j}$, for $i = j = 1, ..., 4$. Other terms in this figure that are not defined yet, will be explained in Section 5.2.1.

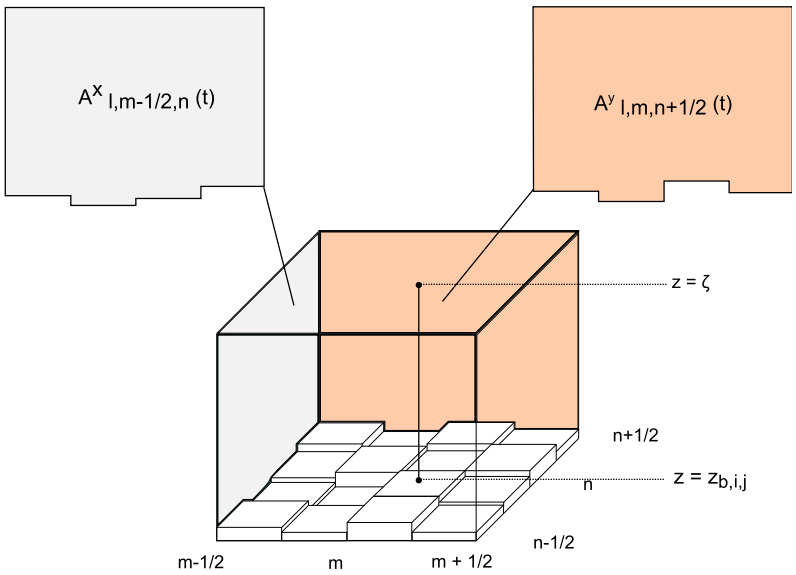

Figure 5.3: Coarse cell with sub-grid

The DEM pixels are the smallest grid cells in the model with a size defined by $\delta x \times \delta x$. Each of the cells are of equal size, while cells of the coarse grid are a multiple of these pixels, see Figure 5.4, where $\Gamma \geq 1$ and $l \geq 0$ are integers. If Figure 5.4 is taken as an example with $l = 2$, then $\Delta x_2 = \Gamma 2^2 \delta x = 4\Gamma \delta x$. Thus, the coarse cell consists of $\Gamma 2^l \times \Gamma 2^l$ DEM pixels. It can be seen from the figure that the cell consist of 8×8 DEM pixels, hence, $\Gamma = 2$ in this example.

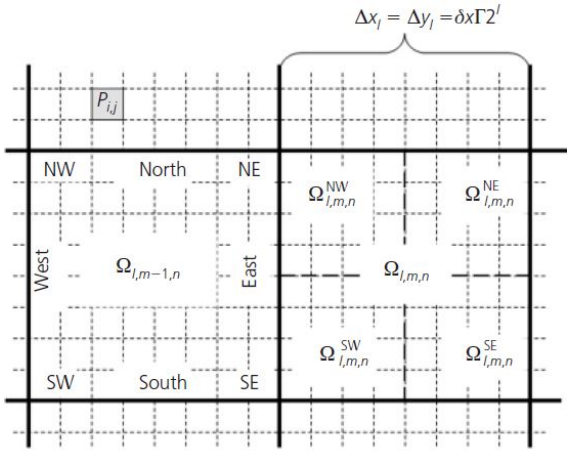

Figure 5.4: Coarse grid sub-domains (Stelling, 2012)

5.2.1 Integration of the grids

The two sub-domains are denoted by Ω for the coarse cell and P for a pixel. Both are continuous domains and they are defined as

$$\begin{aligned} P_{i,j} &= [(i-1)\delta x, i\delta x] \times [(j-1)\delta x, j\delta x] \\ \Omega_{l,m,n} &= [(m-1)\Delta x_l, m\Delta x_l] \times [(n-1)\Delta x_l, n\Delta x_l]. \end{aligned} \tag{5.1}$$

In order to integrate both grids with each other step functions that are based on a indicator function χ_D are defined.

$$\chi_D(x,y) = \begin{cases} 1 & \text{if } (x,y) \in D \\ 0 & \text{if } (x,y) \notin D \end{cases} \tag{5.2}$$

With these definitions, functions of the bottom z_b, water level ζ and water depth h can be approximated. Note that the approximated functions can be recognized by the tilde.

$$z_b(x,y) \approx \tilde{z}_b(x,y) = \sum_{i=1}^{I} \sum_{j=1}^{J} z_{b,i,j} \chi_{P_{i,j}}(x,y) \tag{5.3}$$

$$\zeta(x,y) \approx \tilde{\zeta}(x,y) = \sum_{m=1}^{M} \sum_{n=1}^{N} \zeta_{l,m,n}(t) \chi_{\Omega_{l,m,n}}(x,y) \tag{5.4}$$

$$h(x,y) \approx \tilde{h}(x,y) = \max[0, \tilde{\zeta}(x,y,t) - \tilde{z}_b(x,y)]. \tag{5.5}$$

Notice the difference between summation of water levels and bottom levels. Whereas the bottom level is defined at each pixel in a coarse cell, the water levels are given at coarse cells. 3Di works with a staggered grid. Hence, the water levels are calculated at the center of a cell while the velocities are calculated at the middle of a edge on the coarse grid. Since it is possible that there are cells of two sizes adjacent to each other, it is meant at the middle of an edge of the smallest cell. Velocity domains also depend on the level difference between two adjacent cells. This can be notated by defining the quarter sub-domains in terms of compass directions, see Figure 5.4.

$$\Omega^{SW}_{l,m,n} = [(m-1)\Delta x_l, (m-1/2)\Delta x_l] \times [(n-1)\Delta y_l, (n-1/2)\Delta y_l] \tag{5.6}$$

$$\Omega^{NW}_{l,m,n} = [(m-1)\Delta x_l, (m-1/2)\Delta x_l] \times [(n-1/2)\Delta y_l, n\Delta y_l] \tag{5.7}$$

$$\Omega^{SE}_{l,m,n} = [(m-1/2)\Delta x_l, m\Delta x_l] \times [(n-1)\Delta y_l, (n-1/2)\Delta y_l] \tag{5.8}$$

$$\Omega^{NE}_{l,m,n} = [(m-1/2)\Delta x_l, m\Delta x_l] \times [(n-1/2)\Delta y_l, n\Delta y_l] \tag{5.9}$$

$$\tag{5.10}$$

If one compares Figure 5.4 with Figure 5.2 it can be seen that the sub-domains in terms of compass directions overlap with the quarter cells at a different level: $\Omega_{l-1,2m+1,2n} =$

$\Omega^{NW}_{l,m+1,n}$, etc. Velocity domains, $\Omega_{l,m+1/2,n}$ or $\Omega_{l,m,n+1/2}$, can be constructed with these quarter cells. Generally,

$$\Omega_{l,m+1/2,n} = \Omega^E + \Omega^W \tag{5.11}$$

where there are multiple options for Ω^E and Ω^W, depending on the level difference between cells.

$$\Omega^E = \begin{cases} \Omega^{NW}_{l+1,m/2+1,n/2} & l^E > l, \quad n = \text{ even} \\ \Omega^{SW}_{l+1,m/2+1,(n+1)/2} & l^E > l, \quad n = \text{ odd} \\ \Omega^{SW+NW}_{l,m+1,n} & l^E = l \end{cases} \tag{5.12}$$

$$\Omega^W = \begin{cases} \Omega^{NE}_{l+1,m/2,n/2} & l^W > l, \quad n = \text{ even} \\ \Omega^{SE}_{l+1,m/2,(n+1)/2} & l^W > l, \quad n = \text{ odd} \\ \Omega^{SE+NE}_{l,m,n} & l^W = l \end{cases} \tag{5.13}$$

where l^E, l^W are the level layer of the cell. If level layers of the adjacent cells are equal, then the number of quarter cells that are used is equal to four. Otherwise, it is equal to three: two quarters of the smallest cell and one quarter of the larger cell. The same steps can be done for $\Omega_{l,m,n+1/2} = \Omega^N + \Omega^S$. Now that the domains are defined it is possible to describe the following discrete variables.

Cross sections in the $x-$ and y-direction respectively (Figure 5.4)

$$A^x_{l,m+1/2,n} = \int_{(n-1)\Delta y_l}^{n\Delta y_l} \tilde{h}(m\Delta x_l, y, t)dy = \delta x \sum_{j=j_0}^{j=j_1} \max(0, {}^*\zeta_{l,m+1/2,n} - z_{b,i+1/2,j}) \tag{5.14}$$

$$A^y_{l,m,n+1/2} = \int_{(m-1)\Delta x_l}^{m\Delta x_l} \tilde{h}(x, n\Delta y_l, t)dx = \delta x \sum_{i=i_0}^{i=i_1} \max(0, {}^*\zeta_{l,m,n+1/2} - z_{b,i,j+1/2}). \tag{5.15}$$

It is allowed to go from the integrals to summations due to the fact that coarse cells are composed of pixels which are simply step functions. Notice the new value ${}^*\zeta_{l,m+1/2,n}$. This is the water depth at the interface. Since it is only defined in the center of a cell first-order upwinding is applied to find this value. Hence, second order errors are obtained.

$${}^*\zeta_{l,m+1/2,n} = \max\left(0, \frac{u_{l,m+1/2,n}}{|u_{l,m+1/2,n}|}\right)\zeta_{l,m,n} - \min\left(0, \frac{u_{l,m+1/2,n}}{|u_{l,m+1/2,n}|}\right)\zeta_{l,m+1,n} + \mathcal{O}(\Delta x_l^2) \tag{5.16}$$

Further, if we look at the cross section in the $x-$direction

$$z_{b,i+1/2,j} = \max(z_{b,i,j}, z_{b,i+1,j}) \tag{5.17}$$

$$i = 2^l \Gamma m \tag{5.18}$$

$$j_0 = 2^l \Gamma (n-1) + 1 \tag{5.19}$$

$$j_1 = 2^l \Gamma n. \tag{5.20}$$

Based on this information elements of the cross section in the $y-$direction should be clear as well.

Volume of water in cell $\Omega_{l,m,n}$:

$$V_{l,m,n}(t) = \int_{\Omega_{l,m,n}} \tilde{h}(x,y,t)d\Omega = \delta x^2 \sum_{i=i_0}^{i=i_1} \sum_{j=j_0}^{j=j_1} \max(0, \zeta_{l,m,n} - z_{b,i,j}). \tag{5.21}$$

in which

$$i_0 = 2^l \Gamma(m-1) + 1 \tag{5.22}$$

$$i_1 = 2^l \Gamma m \tag{5.23}$$

and j_1, j_0 as defined in (5.19) and (5.20).

Volume of water in a velocity domain $\Omega_{l,m+1/2,n}$:

$$\begin{aligned} V_{l,m+1/2,n}(t) &= \int_{\Omega_{l,m+1/2,n}} \tilde{h}(x,y,t)d\Omega \\ &= \int_{\Omega^E} \tilde{h}(x,y,t)d\Omega + \int_{\Omega^W} \tilde{h}(x,y,t)d\Omega \end{aligned} \tag{5.24}$$

where Ω^E, Ω^W are defined in (5.12) and (5.13). This summation is not the same as for the volume cell $\Omega_{l,m,n}$, where just one water level $\zeta_{l,m,n}$ is needed. In this case the summation consists of two parts, where summation of the east cell is done with the water level $\zeta_{l,m,n}$, while for the west cell it is done with the water level $\zeta_{l,m+1,n}$.

Volume-averaged velocity:

$$u_{l,m+1/2,n} \approx \frac{\int_{\Omega_{l,m+1/2,n}} u(x,y,t)h(x,y,t)d\Omega}{\int_{\Omega_{l,m+1/2,n}} h(x,y,t)d\Omega} \tag{5.25}$$

Discharge:

$$Q^x_{l,m+1/2,n}(t) = A^x_{l,m+1/2,n}(t) u_{l,m+1/2,n}(t) \tag{5.26}$$

$$Q^y_{l,m,n+1/2}(t) = A^y_{l,m,n+1/2}(t) u_{l,m,n+1/2}(t) \tag{5.27}$$

Now that everything is defined, the shallow water equations can be discretized in the next section.

5.3 Discretisation of the shallow water equations

The shallow water equations are discretized with the finite volume method (FVM). The mesh over which spatial discretization is performed was already defined in the previous sections. In each cell of this mesh the integrals are approximated by the discrete variables that were described in Section 5.2.1. With each time step these variables are modified. The following sections treat the spatial discretization and time discretization.

5.3.1 Spatial discretisation

First of all the shallow water equations are rewritten for just one cell Ω. In case of the continuity equation this cell of interest is $\Omega_{l,m,n}$, whereas for the momentum equations this is the velocity domain $\Omega_{l,m+1/2,n}$.

$$(V_{l,m,n})_t + \sum_f Q\mathbf{n}_f = 0, \tag{5.28}$$

the continuity equation with f the faces of $\Omega_{l,m,n}$ and $\mathbf{n}_f$ the outward directed normal for a face. The number of faces, hence discharges, is dependent on the ordering of local quadtrees. Looking at a velocity domain $\Omega_{l,m+1/2,n}$ the momentum equation in the $x-$direction is given by

$$(uV)_t + \sum_{\delta\Omega} {}^*u\bar{Q}\mathbf{n}_f + \int_\Omega \tilde{h}g\frac{\partial\zeta}{\partial x}d\Omega + \int_\Omega \frac{\tau_b^u}{\rho}d\Omega = 0 \tag{5.29}$$

which is in conservative form. The first term can be simplified by rewriting $(uV)_t = u_tV + uV_t$. Substituting into the above equation, dividing by V and letting $\hat{\tau} = \tau/\rho$ the following equation is obtained from the conservative momentum equation,

$$u_t + \frac{1}{V}\left(\sum_{\delta\Omega} {}^*u\bar{Q}\mathbf{n}_f + uV_t\right) + \frac{1}{V}\left(\int_\Omega \tilde{h}g\frac{\partial\zeta}{\partial x}d\Omega\right) + \frac{1}{V}\left(\int_\Omega \frac{\tau_b^u}{\rho}d\Omega\right) = 0 \tag{5.30}$$

for $\Omega_{l,m+1/2,n}$. Note that there is a new velocity ${}^*u$ appearing in the equation. This is the velocity on the edge of a velocity domain. These edges are different from the edges where velocity is defined. So, they are computed by upwinding. The terms between the brackets are from left to right known as advection, pressure (hydrostatic) and bottom friction. Each of them is discretized separately in the following parts.

Hydrostatic pressure

Starting with the hydrostatic pressure, it is assumed that the pressure gradient $\frac{\partial\zeta}{\partial x}$ is constant. Hence, between the water levels calculated at the center of the coarse cell a linear relation is assumed.

$$\begin{aligned}\frac{-F_{hp}^x}{V} &= \frac{\int_\Omega \tilde{h}g\frac{\partial\zeta}{\partial x}d\Omega}{V} \\ &= \frac{g\frac{\partial\zeta}{\partial x}\int_\Omega \tilde{h}d\Omega}{V} \\ &= g\frac{\partial\zeta}{\partial x} = g\frac{\zeta^E - \zeta^W}{(\Delta^E + \Delta^W)/2}.\end{aligned} \tag{5.31}$$

The values of ζ^E, ζ^W depend on the level difference between the two adjacent cells. In case of the same level $l^E = l^W$

$$\zeta^E = \zeta_{l,m+1,n}, \quad \zeta^W = \zeta_{l,m,n}. \tag{5.32}$$

If there is a difference in the level layer it gets a bit more complicated. If $l^E > l^W$ then the following two options are possible,

$$\zeta^E = \begin{cases} \zeta_{l+1,m/2+1,n/2}, & n = \text{ even} \\ \zeta_{l+1,m/2+1,(n+1)/2}, & n = \text{ odd} \end{cases}, \quad \zeta^W = \begin{cases} \frac{1}{2}(\zeta_{l,m,n} + \zeta_{l,m,n-1}), & n = \text{ even} \\ \frac{1}{2}(\zeta_{l,m,n} + \zeta_{l,m,n+1}), & n = \text{ odd} \end{cases} \tag{5.33}$$

When $l^E < l^W$ the following water levels are used,

$$\zeta^E = \begin{cases} \frac{1}{2}(\zeta_{l,m+1,n} + \zeta_{l,m+1,n-1}), & n = \text{ even} \\ \frac{1}{2}(\zeta_{l,m+1,n} + \zeta_{l,m+1,n+1}), & n = \text{ odd} \end{cases}, \quad \zeta^W = \begin{cases} \zeta_{l+1,m/2,n/2}, & n = \text{ even} \\ \zeta_{l+1,m/2,(n+1)/2}, & n = \text{ odd} \end{cases} \tag{5.34}$$

Advection

The advection term is given by

$$-\hat{F}^x_{adv} = \sum_f {}^*u\bar{Q}\mathbf{n}_f + uV_t. \tag{5.35}$$

As said before, ${}^*u$ represents velocities on edges of the velocity cell which are computed by upwinding. It remains to find a way to compute the discharges $\bar{Q}$ at the faces of a velocity domain. Figure 5.5 shows discharges at the faces of such a cell. In this cell the mass conservation law has to be fulfilled.

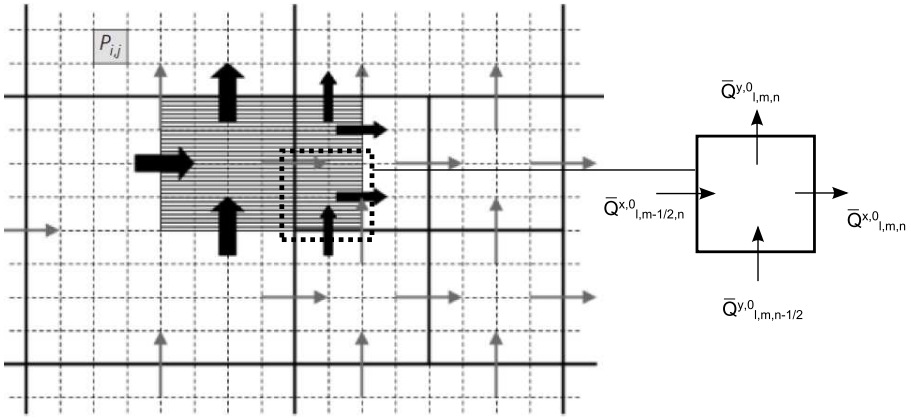

Figure 5.5: Discharges for momentum transport (Stelling, 2012)

Not all discharges at the faces of sub-volumes are known. It is known that each velocity domain consists of three or four quarters of sub-volumes. For each of these sub-volumes a mass-continuity equation is used to compute the sub-grid discharges.

$$(V^{SW}_{l,m,n})_t = \bar{Q}^{x,0}_{l,m-1/2,n} - \bar{Q}^{x,0}_{l,m,n} + \bar{Q}^{y,0}_{l,m,n-1/2} - \bar{Q}^{y,0}_{l,m,n} \tag{5.36}$$

where $\bar{Q}^{x,0}_{l,m-1/2,n}, \bar{Q}^{y,0}_{l,m,n-1/2}$ are the external discharges and the other two internal discharges of $V_{l,m,n}$. The external discharges are computed by assuming

$$\bar{u}^0_{m-1/2,n} = \bar{u}^1_{m-1/2,n} = u_{m-1/2,n} \tag{5.37}$$

such that

$$\bar{Q}^{x,1}_{l,m-1/2,n} = u_{l,m-1/2,n} A^{x,1} = u_{l,m-1/2,n} \int_{(n-1/2)\Delta y_l}^{n\Delta y_l} \tilde{h}\left((m-1)\Delta x_l, y, t\right) dy. \tag{5.38}$$

The same can be done for the other external discharge. The problem in computing discharges lies in the internal discharges. Using Equation (5.36) for all sub-volumes of $\Omega_{l,m,n}$ four equations are obtained with the four unknown internal discharges. The resulting system does not have a unique solution however. Stelling (2012) solved this by replacing one of the four equations by a requirement. Which is that the following expression should be minimal at (l, m, n),

$$E_Q = \left(\frac{\bar{Q}^{x,0}}{A^{x,0}}\right)^2 + \left(\frac{\bar{Q}^{x,1}}{A^{x,1}}\right)^2 + \left(\frac{\bar{Q}^{y,0}}{A^{y,0}}\right)^2 + \left(\frac{\bar{Q}^{y,1}}{A^{y,1}}\right)^2. \tag{5.39}$$

Once the fourth equation is replaced by this equation the solution can be attained by a linear least-squares method. Advection of momentum can now be written as

$$-\hat{F}^x_{adv} = \sum_f {}^*u\bar{Q}\mathbf{n}_f + uV_t = \sum_f ({}^*u - u)\bar{Q}\mathbf{n}_f. \tag{5.40}$$

The summation will consist of inflowing momentum only. For outflowing momentum the value for ${}^*u$ is equal to u when first-order upwinding is used. Furthermore, it is assumed that the flow is hydrostatic, hence, in case of strong contractions in the flow there will be errors. To counter these errors a correction has to be applied that is thought of by Stelling and Duinmeijer (2003). The advection term can now be written as

$$adv(u) = \frac{1}{V} \sum_f ({}^*u - u)\bar{Q}\mathbf{n}_f \tag{5.41}$$

Bottom friction

The last term that needs to be discretized is the bottom friction force $\hat{F}^x_{bot}$.

$$-\hat{F}^x_{bot} = \int_\Omega \frac{\tau^u_b}{\rho} d\Omega = \int_\Omega c^f u \|u\| d\Omega \tag{5.42}$$

The cell of interest is still $\Omega_{l,m+1/2,n}$, since the momentum equations is defined on this cell. The velocity in this cell is not known, except at $(l, m+1/2, n)$. It is possible to assume a constant velocity in the entire cell. However, looking at shallow flows that can contain locally relative deep parts this will lead to deviation in gravity-driven flows. It leads to an overestimation of the velocity, hence friction, and an underestimation of conveyance. The following assumptions are done to find a function $\tilde{u}(x, y)$.

Note, these assumptions are not valid when instead of gravity the flow is driven dominantly by wind.

In each quarter of a computational cell it is assumed that the friction slope S^f, rate at which energy is lost along a given length of channel, is constant. Second, a constant direction of the flow is taken. These assumptions are done in order to keep the computational time small. Without these assumptions one would need to compute each velocity for a pixel one by one. Of course, this would be very expensive. Since the flow is gravity-driven the dominant terms in the momentum equation are the pressure term and friction term. These terms are used to compose an expression for the friction slope for a quarter cell $\Omega = \Omega^{SW,\ldots,NE}_{l,m,n}$,

$$|S^f| = \frac{c^f \|\tilde{u}\|^2}{g\tilde{h}} = \text{constant if } (x, y) \in \Omega \tag{5.43}$$

with $\tilde{h} = \tilde{h}(x, y)$, the water depth that depends on the water and bottom level at point (x, y). The following velocity is one calculated within a quarter of a computational cell. Hence at SW,..., NE of (l, m, n).

$$\|\tilde{u}\| = \frac{1}{V} \int_\Omega \tilde{h}(\tilde{u}(x, y)^2 + \tilde{v}(x, y)^2)^{1/2} dxdy = \frac{1}{V} \int_\Omega \tilde{h} \|\tilde{u}(x, y)\| dxdy \tag{5.44}$$

where the velocity inside the integral is a cell varying velocity, while the one being calculated is a cell average velocity of a quarter cell. If two points $(x, y), (x', y')$ are taken, both in Ω, then

$$\frac{c^f(x, y)(\tilde{u}(x, y)^2 + \tilde{v}(x, y)^2)}{g\tilde{h}(x, y)} = \frac{c^f(x', y')(\tilde{u}(x', y')^2 + \tilde{v}(x', y')^2)}{g\tilde{h}(x', y')}, \tag{5.45}$$

so

$$\|\tilde{u}(x, y)\| = \|\tilde{u}(x', y')\| \left(\frac{c^f(x', y')}{\tilde{h}(x', y')} \right)^{1/2} \left(\frac{\tilde{h}(x, y)}{c^f(x, y)} \right)^{1/2}. \tag{5.46}$$

Both assumptions are used to come to this expression. That is why it is only valid when both points are inside the same cell. A last assumption that is made is

$$\|\tilde{u}(x', y')\| = \frac{\|u\|}{\alpha(x', y')} \tag{5.47}$$

with u the calculated velocity on the edge of a cell. If, for example, $\Omega = \Omega^{NW}_{l,m,n}$, then

$$u = u^{NW}_{l,m,n} = \begin{cases} u_{l,m-1/2,n} \\ \text{or} \\ u_{l-1,2m-3/2,2n} \end{cases} \tag{5.48}$$

$$v = v^{NW}_{l,m,n} = \begin{cases} v_{l,m,n+1/2} \\ \text{or} \\ v_{l-1,2m-1,2n+1/2} \end{cases} . \tag{5.49}$$

Working out α' which is used in the final step to obtain the bottom friction,

$$\begin{aligned} \alpha' &= \frac{\|u\|}{\|\tilde{u}'\|} = \frac{\int_\Omega \|\tilde{u}\|\tilde{h}dxdy}{\|\tilde{u}'\|V} \\ &= \frac{\|\tilde{u}'\| \int_\Omega \tilde{h}(\tilde{h}/c^f)^{1/2}dxdy}{\|\tilde{u}'\|V(\tilde{h}'/c^{f'})^{1/2}} \\ &= \frac{\int_\Omega \tilde{h}(\tilde{h}/c^f)^{1/2}dxdy}{V} \left(\frac{c^{f'}}{\tilde{h}'}\right)^{1/2} \end{aligned} \tag{5.50}$$

where $c^{f'} = c^f(x', y')$, $\tilde{h}' = \tilde{h}(x', y')$, $\alpha' = \alpha(x', y')$. Now the bottom friction can be defined with the function $\tilde{u}(x, y)$ instead of a constant velocity in the entire cell.

$$-\hat{F}^x_{bot} = \int_\Omega \frac{\tau^u_b}{\rho} d\Omega = \int_\Omega c^f \tilde{u}\|\tilde{u}\| d\Omega. \tag{5.51}$$

Substituting Equation (5.47) and subsequently writing out α by using Equation (5.50) the bottom friction is now defined by

$$\begin{aligned} -\hat{F}^x_{bot} &= \int_\Omega c^f \tilde{u}\|\tilde{u}\| d\Omega = u\|u\| \int_\Omega \frac{c^f}{\alpha^2} dxdy \\ &= u\|u\| \int_\Omega \frac{c^f}{c^f \cdot \left(\int_\Omega \tilde{h}(\tilde{h}/c^f)^{1/2}dxdy\right)^2} V^2 \tilde{h} dxdy \\ &= u\|u\| \frac{V^3}{\left(\int_\Omega \tilde{h}(\tilde{h}/c^f)^{1/2}dxdy\right)^2} \end{aligned} \tag{5.52}$$

for a quarter cell $\Omega = \Omega_{l,m,n}^{SW,\ldots,NE}$. For a velocity domain the friction force will be the sum of all quarter sub-domains. If $l^E = l^W$, then four quarter sub-domains are taken. Otherwise, only three quarter sub-domains. This was already explained in Section 5.2.1. Suppose that the levels of adjacent cells are equal, then

$$\begin{aligned} -\left(\frac{\hat{F}_{bot}^x}{V}\right)_{l,m+1/2,n} &= \frac{(\hat{F}_{bot}^x)_{l,m+1/2,n}^{W+E}}{-V_{l,m+1/2,n}} \\ &= \frac{(F_{bot}^x)_{l,m,n}^{NE+SE} + (F_{bot}^x)_{l,m+1,n}^{NW+SW}}{-V_{l,m+1/2,n}} \\ &= \frac{u_{l,m+1/2,n}}{V_{l,m+1/2,n}} \left(f_{l,m,n}^{NE+SE} + f_{l,m+1,n}^{NW+SW}\right) \end{aligned} \tag{5.53}$$

with f defined as a friction factor and h^f as the roughness depth.

$$f = V\frac{\|u\|}{h^f}, \qquad h^f = \left[\frac{\int_\Omega \tilde{h}(\tilde{h}/c^f)^{1/2}dxdy}{V}\right]^2. \tag{5.54}$$

Using this friction factor makes it very easy to compute the bottom friction force. For each sub-domain the friction factor is computed, which can also be used for the force in $y-$direction. It might look like this way uses a lot of memory.

5.3.2 Time discretisation

Discretisation in time is done with the semi-implicit theta method. For the bottom friction some predictor-corrector is also applied, which is necessary to model large-area flooding problems (Stelling, 2012). Respectively for the continuity and momentum equations the time integration is as follows,

$$\frac{V(\zeta^{k+1}) - V(\zeta^k)}{\Delta t} + \sum_f A^k u^{k+\theta} \mathbf{n}_f = 0 \text{ at } (l,m,n) \tag{5.55}$$

$$\frac{u^{k+1} - u^k}{\Delta t} + \text{adv}(u^k) + g\frac{\partial \zeta^{k+\theta}}{\partial x} + \frac{u^{k+1}}{V(\zeta^k)}(f^k)^{E+W} = 0 \text{ at } (l,m+1/2,n)(l^E = l^W) \tag{5.56}$$

with $p^{k+\theta} = (1-\theta)p^k + \theta p^{k+1}$ and $\theta \in [\frac{1}{2}, 1]$ (Casulli, 2009). If the level layers are not the same, the pressure gradient takes another form. Describing the hydrostatic pressure term in Section 5.3.2, it is seen that there are four other possibilities, see (5.34) and (5.35). One of these pressure terms, $l^W > l^E$ is taken with $n =$ even, is taken as an example at the end of this section. Solving the equations u^{k+1} has to be eliminated from the mass

conservation equation. Taking the case $l^E = l^W$ as an example, Equation (5.56) has to be rewritten such that an expression for u^{k+1} is found.

$$u^{k+1} = \frac{1}{B}\left(u^k - \Delta t(adv(u^k) + g\frac{\partial \zeta^{k+\theta}}{\partial x})\right) \tag{5.57}$$

with

$$B = 1 + \frac{\Delta t}{V(\zeta^k)}(f^k)^{E+W}. \tag{5.58}$$

Substituting this into the mass equation results in

$$\begin{aligned} V(\zeta^{k+1}) - g\Delta t^2\frac{\theta^2}{B}\sum_f \frac{\partial \zeta^{k+1}}{\partial x}A^k\mathbf{n}_f =& V(\zeta^k) - \Delta t\sum_f A^k\mathbf{n}_f\left[\theta\frac{\Delta t}{B}\left(adv(u^k) + ..\right.\right. \\ & \left.\left.. + g(1-\theta)\frac{\partial \zeta^k}{\partial x}\right) + (1-\theta)u^k\right]. \end{aligned} \tag{5.59}$$

This equation can be written in a vector notation

$$\mathbf{V}(\zeta) + \mathbf{T}\zeta = \mathbf{b} \tag{5.60}$$

which is solved by an iterative scheme where it is assured that the system converges under physically compatible assumptions (Casulli, 2009). This is done based on a Newton iteration. Note that the system in nonlinear because of the water volumes (defined at ...). The water volume V is assumed strictly positive, since a value of zero would lead to the trivial solution.

When $l^E \neq l^W$ the system differs in the pressure terms as seen before. If $l^W > l^E$ is taken with $n =$ even, then the pressure term is

$$\begin{aligned} \frac{\partial \zeta}{\partial x} &= \frac{\frac{1}{2}(\zeta_{l,m+1,n} - \zeta_{l,m+1,n-1}) - \zeta_{l+1,m/2,n/2}}{\frac{1}{2}(\Delta x_{l+1} + \Delta x_l)} \\ &= \frac{\zeta_{l,m+1,n-1} - \zeta_{l,m+1,n}}{\Delta x_{l+1} + \Delta x_l} + \frac{\zeta_{l,m+1,n} - \zeta_{l+1,m/2,n/2}}{\frac{1}{2}(\Delta x_{l+1} + \Delta x_l)} = \frac{\partial \zeta}{\partial x} - d_y\zeta + d_y\zeta. \end{aligned} \tag{5.61}$$

The term $d_y\zeta$ is added to avoid stability problems. The difference with Equation (5.56) can be seen if the time integrations are compared. For the latter the time integration is given by

$$\frac{u^{k+1} - u^k}{\Delta t} + \mathrm{adv}(u^k) + g(\frac{\partial}{\partial x} - d_y)\zeta^{k+\theta} + gd_y\zeta^k + \frac{u^{k+1}}{V(\zeta^k)}(f^k)^{E+W} = 0. \tag{5.62}$$

If n = odd, then

$$\frac{u^{k+1}-u^k}{\Delta t} + \text{adv}(u^k) + g(\frac{\partial}{\partial x} + d_y)\zeta^{k+\theta} - gd_y\zeta^k + \frac{u^{k+1}}{V(\zeta^k)}(f^k)^{E+W} = 0. \tag{5.63}$$

It can be seen that the plus and minus sign are different for the pressure term. This gives that their arises anti-symmetry in the system which avoids stability problems due to the explicit $d_y\zeta$ term. This system is solved with a method that combines the Conjugate Gradient method and Gaussian elimination.

Chapter 6

Description of the problem

6.1 Research questions

Both the programs 3Di and D-Flow Flexible Mesh are quite new and came available around the same time. This gives that when making a decision between the usage of one or another it is not clear what to choose. Most of the time a random decision is taken, or one chooses their preference. Knowing which of the two programs to use in certain projects can lead to preciser results, hence, a better model.

The general research question will be

"What needs to be considered when modeling 2DH in either D-Flow Flexible Mesh or 3Di?"

This thesis is a combination of both the master Applied Mathematics and Hydraulic Engineering. Hence, it should fulfill the requirements for both masters. The thesis will be split into two parts. In the first part the focus is more on a mathematical objective, while the second part zooms deeper in on a fluid mechanical question. Both parts distinguish D-Flow Flexible Mesh and 3Di, so the conclusions can be used to answer the general research question.

The objective of the first part of the thesis is to find out how large the discretisation errors when refining can be in both the grid of Flexible Mesh and 3Di. It is of importance to know how well the results are in comparison with the reality. Making a refinement often means that the local area is interesting to model, hence, the errors should be small. This has led to the following research question:

"How do local grid refinements influence the modeling results of river hydrodynamics?"

with subquestions

- How are the grids refined?

- Are the results depended on the grid itself?
- What are the errors due to the numerical approximation?
- What is the amount of work needed to do these refinements?

The second part will take a look at the modeling of physical aspects. Flexible Mesh has the possibility to model both 3D and 2DH. However, 3Di can only model in 2DH. Hence, the models are implemented as 2DH. As a result, the modeled physical aspect might contain large errors at places where 3D processes are significant. This led to the following research question:

"Which processes are determinative for the suitability of D-Flow Flexible Mesh or 3Di with a specific problem?"

with subquestions

- What assumptions are done to go from 3D to 2DH?
- What are the consequences of these assumptions?
- What are the errors in models due to the assumptions?
- If the results differ in both models, where do these differences come from?

In the following section some test models are described that will help to understand the processes. Eventually a whole river will be modeled.

6.2 Test models

In order to get a better understanding of what the programs are capable of, some test models are set up. These test models are the preparing steps to model (part of) a river.

6.2.1 Straight channel with rectangular cross section

In the validation document of Deltares for Flexible Mesh convergence is tested for straight channels with a rectangular cross section. This will not be repeated in this thesis. However, this simple test model is good to start with and learn how to use both programs. Insight that is gained with this model can be used for the models that follow. It is possible to add a fixed weir over part of the width or the whole width to see how this affect the flow.

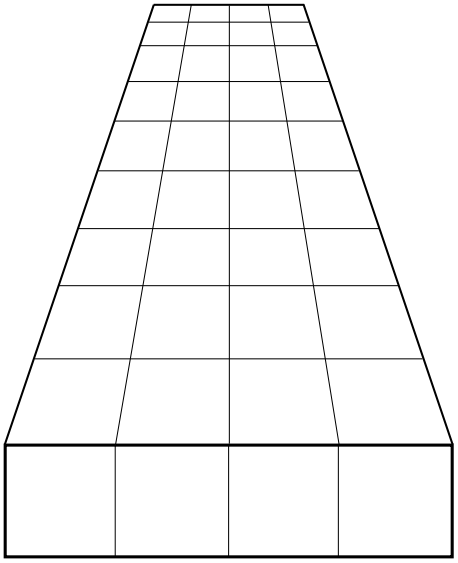

Figure 6.1: Straight channel with rectangular cross section

6.2.2 U-bend

Another test model is the U-bend. Rivers are never just straight channels, hence, it is important to understand what is happening in bends. In this case both programs differ in how they model bends. 3Di will represent this bend in a staircase boundary, while Flexible Mesh has the possibility to follow the bend with its grid. For 3Di it will be interesting how this is done, since storage of water is done on subgrid level while pressure terms are solved on a coarse grid.

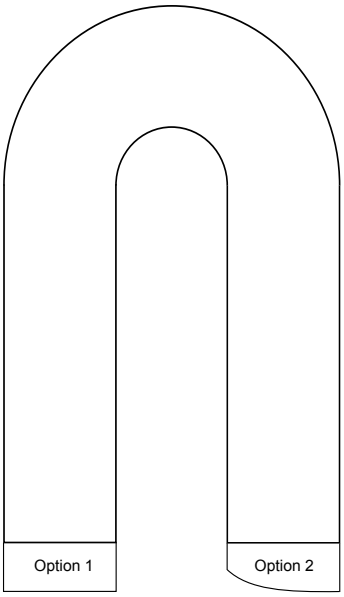

Figure 6.2: U-bend

Modeling this test model will be harder than the one after this. However, it is expected

that it will give much insight in the storage and how velocities are behaving. For the cross section two options will be used. A simple rectangular cross section to start with, followed by a sinusoidal cross section, see Figure 6.2. Of course, option two is more realistic.

6.2.3 Straight channel with trapezoidal cross section

The final test model will again be a straight channel. However, it differs from the first model by the cross section. Whereas the first had a rectangular cross section, this model will have a trapezoidal cross section. In rivers it is more realistic that the sides have a slope. For this case convergence is not tested yet. Thus, the first step will be to perform such a convergence test. This will show how it behaves for different grid resolutions. Once this is done it will be easier to understand the results of local grid refinement. Thus, step two will be to apply local grid refinement in multiple ways. For Flexible Mesh this means it can be done as in Figure 6.3. Another possibility is to apply only triangles after the refinement. For 3Di there is only one option. Recall this from Chapter 5.

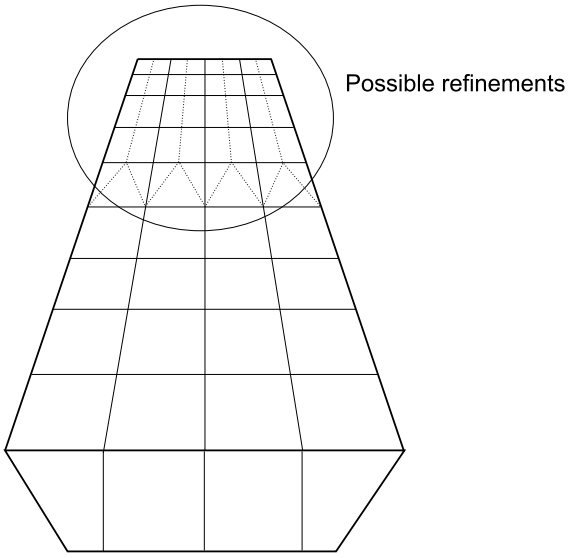

Figure 6.3: Straight channel with trapezoidal cross section

Modeling a trapezoidal cross section gives that is also matters which type of conveyance is used in Flexible Mesh, see Section 4.1.2. So these types should be compared with each other. The final step in this model is to add fixed weirs.

6.2.4 River Elbe

The real study is done for the river Elbe. The BAW is a central institute in Germany for Hydraulic Engineering. A while back they completed a project at the Elbe where room for the river was made by replacing the dike. The old dike was broken through at a few points where the water could get through. Lots of measurements where done at multiple places, see figure below. These measurements can be used to validate both models in 3Di and Flexible Mesh. At points where measurements were done, local grid refinements

will be applied. This gives that hopefully a good comparison can be made. Further, the processes around and at the groynes will be examined. If it is possible, also the processes at the inlet in the dike will be examined. However, this depend on the time.

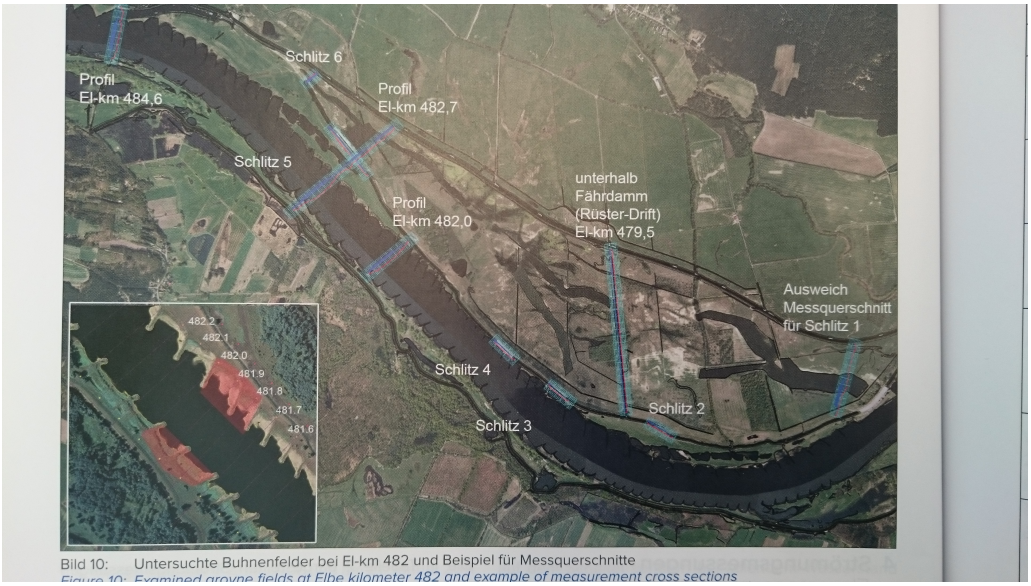

(a) Model area

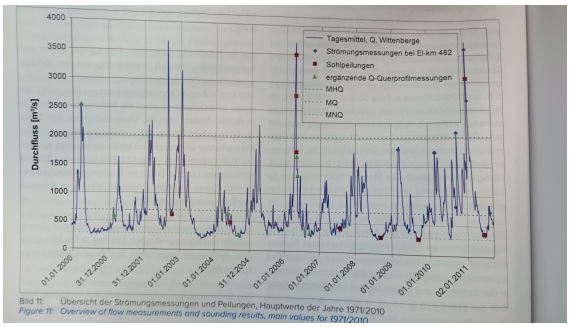

(b) Discharge river

Figure 6.4: River Elbe

Bibliography

Borsboom, M. (2013). Construction and analysis of D-FLOW FM-type discretizations. Tech. rep., Deltares Memorandum.

Casulli, V. (2009). A high-resolution wetting and drying algorithm for free-surface hydrodynamics. *International Journal for Numerical Methods in Fluids*, 60: 391–408.

Chatterjee, A. (2004). Novel multi-block strategy for CAD tools for microfluidics type applications. *Advances in Engineering Software*, 35: 443–451.

Deltares (2015). *Delft3D Flexible Mesh Suite: D-Flow Flexible Mesh Technical Reference.* Delft.

Hagen, E. T. (2014). *Hydrodynamic river modelling with D-Flow Flexible Mesh.* M.Sc. Thesis, University of Twente.

Ji, Z.-G. (2008). *Hydrodynamics and water quality: modeling rivers, lakes and estuaries.* Cambridge Aerospace Series. Cambridge University Press, Cambridge.

Jirka, G. H. and Uijttewaal, W. S. J. (2004). *Shallow Flows.* Balkema, Leiden.

Kernkamp, H. W. J., van Dam, A., Stelling, G. S., and de Goede, E. D. (2011). Efficient scheme for the shallow water equations on unstructured grids with application to the Continental Shelf. *Ocean Dynamics*, 61: 1175–1188.

Liseikin, V. D. (2004). *A computational differential geometry approach to grid generation.* Springer-Verlag, Berlin.

Perot, B. (2000). Conservation properties of unstructured staggered mesh schemes. *Journal of Computational Physics*, 159: 58–89.

Stelling, G. (2012). Quadtree flood simulations with sub-grid digital elevation methods. *Water Management*, 165: 567–580.

Stelling, G. S. and Duinmeijer, S. P. A. (2003). A staggered conservative scheme for every Froude number in rapidly varied shallow water flows. *International Journal for Numerical Methods in Fluids*, 43(12): 1329–1354.

Uijttewaal, W. S. J. (2015). Turbulence in hydraulics. Lecture Notes.

Vreugdenhil, C. B. (1994). *Numerical Methods for Shallow-Water Flow*. Kluwer Academic Publishers, Dordrecht.

Wang, J. P., Borthwick, A. G. L., and Taylor, R. E. (2004). Finite-volume type VOF method on dynamically adaptive quadtree grids. *International Journal for Numerical Methods in Fluids*, 45(5): 1–22.

Appendix A

Derivation of mass and momentum equations

In this appendix the full derivation of both the conservation of mass and momentum is given. It starts in both cases with a small cubic fluid particle as given in Figure A.1 with forces working on the faces and in- and outgoing fluxes in all three directions.

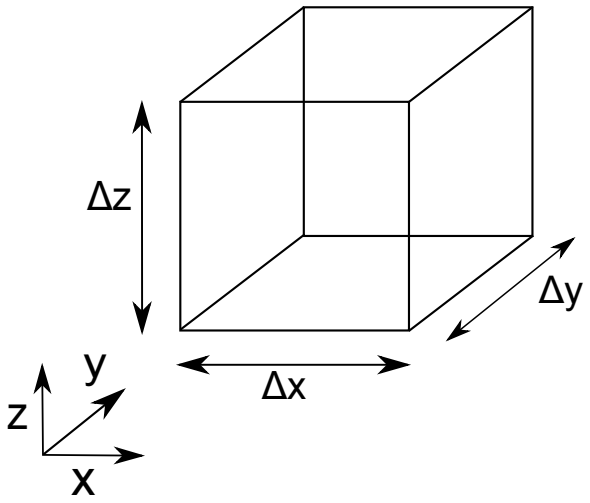

Figure A.1: Fluid particle

A.1 Conservation of mass

A mass balance for a fluid particle is the basic point for the derivation of the mass-conservation equation.

Rate of change of mass in fluid particle = Ingoing flux of mass - Outgoing flux of mass

The rate of change of mass of the fluid particle in Figure can be written as

$$\frac{\rho\Delta x\Delta y\Delta z|_{t+\Delta t} - \rho\Delta x\Delta y\Delta z|_t}{\Delta t} \tag{A.1}$$

The net flux are given as "ingoing flux - outgoing flux"

$$\begin{aligned} x-\text{direction: } & \rho\Delta y\Delta z u|_x - \rho\Delta y\Delta z u|_{x+\Delta x} \\ y-\text{direction: } & \rho\Delta x\Delta z v|_y - \rho\Delta x\Delta z v|_{y+\Delta y} \\ z-\text{direction: } & \rho\Delta x\Delta y w|_z - \rho\Delta x\Delta y w|_{z+\Delta z} \end{aligned} \tag{A.2}$$

Together this gives the mass balance

$$\begin{aligned} \frac{\rho\Delta x\Delta y\Delta z|_{t+\Delta t} - \rho\Delta x\Delta y\Delta z|_t}{\Delta t} =& \rho\Delta y\Delta z u|_x - \rho\Delta y\Delta z u|_{x+\Delta x} + ... \\ & ... + \rho\Delta x\Delta z v|_y - \rho\Delta x\Delta z v|_{y+\Delta y} + ... \\ & ... + \rho\Delta x\Delta y w|_z - \rho\Delta x\Delta y w|_{z+\Delta z} \end{aligned} \tag{A.3}$$

Dividing by $\Delta x, \Delta y, \Delta z$

$$\frac{\rho|_{t+\Delta t} - \rho|_t}{\Delta t} = \frac{\rho u|_x - \rho u|_{x+\Delta x}}{\Delta x} + \frac{\rho v|_y - \rho v|_y + \Delta y}{\Delta y} + \frac{\rho w|_z - \rho w|_z + \Delta z}{\Delta z} \tag{A.4}$$

The final step is taking the limit of $\Delta x, \Delta y, \Delta z, \Delta t$, which gives us the mass-continuity equation.

$$\lim_{\Delta x,\Delta y,\Delta z,\Delta t\to 0} \frac{\rho|_{t+\Delta t} - \rho|_t}{\Delta t} = \lim_{\Delta x,\Delta y,\Delta z,\Delta t\to 0} \left(\frac{\rho u|_x - \rho u|_{x+\Delta x}}{\Delta x} + \frac{\rho v|_y - \rho v|_{y+\Delta y}}{\Delta y} + \frac{\rho w|_z - \rho w|_{z+\Delta z}}{\Delta z} \right) \tag{A.5}$$

$$\frac{\partial \rho}{\partial t} + \frac{\partial \rho u}{\partial x} + \frac{\partial \rho v}{\partial y} + \frac{\partial \rho w}{\partial z} = 0 \tag{A.6}$$

A.2 Conservation of momentum

The basic of the momentum equations is the second law of Newton, $F = m \cdot a$, where m is mass and a acceleration. The first is equal to density times the volume of the element, while the latter is equal to the Laplace derivative.

$$\rho\Delta x\Delta y\Delta z \frac{D\mathbf{v}}{Dt} = \text{sum of forces on element} \tag{A.7}$$

Looking in the x-direction, the sum of forces consist of the net pressure force and the viscous force, also known as the surface forces. The same forces work in the y-direction and the z-direction. Besides the surface forces, there are also body forces like gravity. The gravitational force is directed downwards, hence only in the z-direction an term for the gravity is found.

When looking at waters at large scales, the Coriolis effect also plays a part in the x- and y-direction. Since a general case is treated, it cannot be neglected. Combining all the terms give the following equations.

$$\begin{aligned}
\rho\Delta x\Delta y\Delta z\frac{Du}{Dt} =&\Delta y\Delta z\left(p|_x - p|_{x+\Delta x}\right) + \rho f v\Delta x\Delta y\Delta z + \Delta y\Delta z\left(\tau_{xx}|_x - \tau_{xx}|_{x+\Delta x}\right) + ... \\
&... + \Delta x\Delta z\left(\tau_{yx}|_y - \tau_{yx}|_{y+\Delta y}\right) + \Delta y\Delta x\left(\tau_{zx}|_z - \tau_{zx}|_{z+\Delta z}\right) \\
\rho\Delta x\Delta y\Delta z\frac{Dv}{Dt} =&\Delta x\Delta z\left(p|_y - p|_{y+\Delta y}\right) - \rho f u\Delta x\Delta y\Delta z + \Delta y\Delta z\left(\tau_{xy}|_x - \tau_{xy}|_{x+\Delta x}\right) + ... \\
&... + \Delta x\Delta z\left(\tau_{yy}|_y - \tau_{yy}|_{y+\Delta y}\right) + \Delta y\Delta x\left(\tau_{zy}|_z - \tau_{zy}|_{z+\Delta z}\right) \\
\rho\Delta x\Delta y\Delta z\frac{Dw}{Dt} =&\Delta x\Delta y\left(p|_z - p|_{z+\Delta z}\right) - \rho g\Delta x\Delta y\Delta z + \Delta y\Delta z\left(\tau_{xz}|_x - \tau_{xz}|_{x+\Delta x}\right) + ... \\
&... + \Delta x\Delta z\left(\tau_{yz}|_y - \tau_{yz}|_{y+\Delta y}\right) + \Delta y\Delta x\left(\tau_{zz}|_z - \tau_{zz}|_{z+\Delta z}\right)
\end{aligned} \tag{A.8}$$

Dividing all three equations by $\Delta x\Delta y\Delta z$ and then taking the limit as is done in the previous section gives

$$\begin{aligned}
\rho\frac{Du}{Dt} &= -\frac{\partial p}{\partial x} + \rho f v + \left[\frac{\partial\tau_{xx}}{\partial x} + \frac{\partial\tau_{yx}}{\partial y} + \frac{\partial\tau_{zx}}{\partial z}\right] \\
\rho\frac{Du}{Dt} &= -\frac{\partial p}{\partial y} - \rho f u + \left[\frac{\partial\tau_{xy}}{\partial x} + \frac{\partial\tau_{yy}}{\partial y} + \frac{\partial\tau_{zy}}{\partial z}\right] \\
\rho\frac{Du}{Dt} &= -\frac{\partial p}{\partial z} - \rho g + \left[\frac{\partial\tau_{xz}}{\partial x} + \frac{\partial\tau_{yz}}{\partial y} + \frac{\partial\tau_{zz}}{\partial z}\right]
\end{aligned} \tag{A.9}$$

The term on the left hand side can be rewritten for all three directions, however, only for the x-direction this is shown.

$$\begin{aligned}
\rho\frac{D\mathbf{v}}{Dt} =&\rho\left(\frac{\partial\rho}{\partial t} + u\frac{\partial u}{\partial x} + v\frac{\partial u}{\partial y} + w\frac{\partial u}{\partial z}\right) \\
=&\frac{\partial\rho u}{\partial t} + \frac{\partial\rho u^2}{\partial x} + \frac{\partial\rho uv}{\partial y} + \frac{\partial\rho uw}{\partial z} - u\left(\frac{\partial\rho}{\partial t} + \frac{\partial\rho u}{\partial x} + \frac{\partial\rho v}{\partial y} + \frac{\partial\rho w}{\partial z}\right) \\
=&\frac{\partial\rho u}{\partial t} + \frac{\partial\rho u^2}{\partial x} + \frac{\partial\rho uv}{\partial y} + \frac{\partial\rho uw}{\partial z}
\end{aligned} \tag{A.10}$$

The final step can be done by using the conservation of mass, equation (A.6). Substituting this in (A.8) gives the equations that represent the conservation of momentum.

$$\begin{aligned}
\frac{\partial \rho u}{\partial t} + \frac{\partial \rho u^2}{\partial x} + \frac{\partial \rho uv}{\partial y} + \frac{\partial \rho uw}{\partial z} &= -\frac{\partial p}{\partial x} + \rho f v + \left[\frac{\partial \tau_{xx}}{\partial x} + \frac{\partial \tau_{yx}}{\partial y} + \frac{\partial \tau_{zx}}{\partial z} \right] \\
\frac{\partial \rho u}{\partial t} + \frac{\partial \rho vu}{\partial x} + \frac{\partial \rho v^2}{\partial y} + \frac{\partial \rho vw}{\partial z} &= -\frac{\partial p}{\partial y} - \rho f u + \left[\frac{\partial \tau_{xy}}{\partial x} + \frac{\partial \tau_{yy}}{\partial y} + \frac{\partial \tau_{zy}}{\partial z} \right] \\
\frac{\partial \rho u}{\partial t} + \frac{\partial \rho wu}{\partial x} + \frac{\partial \rho wv}{\partial y} + \frac{\partial \rho w^2}{\partial z} &= -\frac{\partial p}{\partial z} - \rho g + \left[\frac{\partial \tau_{xz}}{\partial x} + \frac{\partial \tau_{yz}}{\partial y} + \frac{\partial \tau_{zz}}{\partial z} \right]
\end{aligned} \tag{A.11}$$

Appendix B

Derivation of the shallow water equations

B.1 RANS equations

The momentum equation in the x-direction is taken as an example for the derivative of the RANS equations.

$$\frac{\partial \rho u}{\partial t} + \frac{\partial \rho u^2}{\partial x} + \frac{\partial \rho uv}{\partial y} + \frac{\partial \rho uw}{\partial z} = -\frac{\partial p}{\partial x} + \rho f v + \left[\frac{\partial \tau_{xx}}{\partial x} + \frac{\partial \tau_{yx}}{\partial y} + \frac{\partial \tau_{zx}}{\partial z}\right] \tag{B.1}$$

Substitute $u = \bar{u} + u'$, $v = \bar{v} + v'$, $w = \bar{w} + w'$, and $p = \bar{p} + p'$ in the momentum equation in the x-direction.

$$\frac{\partial \rho(\bar{u} + u')}{\partial t} + \frac{\partial \rho(\bar{u} + u')^2}{\partial x} + \frac{\partial \rho(\bar{u} + u')(\bar{v} + v')}{\partial y} + \frac{\partial \rho(\bar{u} + u')(w = \bar{w} + w')}{\partial z} = -\frac{\partial \bar{p} + p'}{\partial x} + ... \tag{B.2}$$
$$... + \rho f(\bar{v} + v') + \nabla \cdot \left(2\mu \nabla^s (\bar{u} + u')\right)$$

The next step is to average this equation. By doing this the following rules are used

$$\overline{\bar{u}} = \bar{u}, \qquad \overline{u'} = 0, \qquad \overline{\bar{u}\bar{v}} = \bar{u}\bar{v}, \qquad \overline{u'v'} \neq 0, \qquad \overline{\bar{u} + u'} = \bar{u} \tag{B.3}$$

Thus, averaging Equation (B.2) and using above rules give the RANS for the x-direction. The same steps can be done for the other directions. These will not be done here.

$$\frac{\partial\overline{\rho(\bar{u}+u')}}{\partial t}+\frac{\partial\overline{\rho(\bar{u}+u')^2}}{\partial x}+\frac{\partial\overline{\rho(\bar{u}+u')(\bar{v}+v')}}{\partial y}+\frac{\partial\overline{\rho(\bar{u}+u')(w=\bar{w}+w')}}{\partial z}=-\frac{\partial\overline{\bar{p}+p'}}{\partial x}+... \tag{B.4}$$

$$...+\overline{\rho f(\bar{v}+v')}+\overline{\nabla\cdot(2\mu\nabla^s(\bar{u}+u'))}$$

$$\frac{\partial\rho(\overline{\bar{u}}+\overline{u'})}{\partial t}+\frac{\partial\rho(\overline{\bar{u}^2}+2\overline{\bar{u}u'}+\overline{u'u'})}{\partial x}+\frac{\partial\rho(\overline{\bar{u}\bar{v}}+\overline{\bar{u}v'}+\overline{\bar{v}u'}+\overline{u'v'})}{\partial y}+\frac{\partial\rho(\overline{\bar{u}\bar{w}}+\overline{\bar{u}w'}+\overline{\bar{w}u'}+\overline{u'w'})}{\partial z}= \tag{B.5}$$

$$-\frac{\partial\overline{\bar{p}}+\overline{p'}}{\partial x}+\rho f(\overline{\bar{v}}+\overline{v'})+\nabla\cdot\left(2\mu\nabla^s(\overline{\bar{u}}+\overline{u'})\right)$$

$$\frac{\partial\rho\bar{u}}{\partial t}+\frac{\partial\rho(\bar{u}\bar{u}+\overline{u'u'})}{\partial x}+\frac{\partial\rho(\bar{u}\bar{v}+\overline{u'v'})}{\partial y}+\frac{\partial\rho(\bar{u}\bar{w}+\overline{u'w'})}{\partial z}=-\frac{\partial\bar{p}}{\partial x}+\rho f\bar{v}+\nabla\cdot(2\mu\nabla^s\bar{u}) \tag{B.6}$$

$$\frac{\partial\rho\bar{u}}{\partial t}+\nabla\cdot(\rho\bar{u}\bar{\mathbf{v}})+\nabla\cdot\left(\rho\overline{u'\mathbf{v}'}\right)=-\frac{\partial\bar{p}}{\partial x}+\rho f\bar{v}+\nabla\cdot(2\mu\nabla^s\bar{u}) \tag{B.7}$$

B.2 Scaling

Applying scaling technique to the vertical momentum equations gives insight in the order of magnitude of all terms. Let the terms x and y be of order L and z of the order H, whereas the velocities u and v are of order U. Using the continuity equations gives the order of the velocity w as follows. Write all components as a dimensionless number (recognized by the tilde) times the order of scale.

$$u=U\tilde{u} \tag{B.8}$$
$$v=U\tilde{v} \tag{B.9}$$
$$w=\alpha\tilde{w} \tag{B.10}$$
$$x=L\tilde{x} \tag{B.11}$$
$$y=L\tilde{y} \tag{B.12}$$
$$z=H\tilde{z} \tag{B.13}$$

where α is an unknown order that needs to be derived. Substituting these terms in the continuity equation gives

$$\frac{U}{L}\frac{\partial\tilde{u}}{\partial\tilde{x}}+\frac{U}{L}\frac{\partial\tilde{v}}{\partial\tilde{y}}+\frac{\alpha}{H}\frac{\partial\tilde{w}}{\partial\tilde{z}}=0 \tag{B.14}$$

The first two terms usually do not cancel one another out, hence, α should be such that the third term is of the same order as the first two. This gives that $\alpha=HU/L$. Now these terms can be substituted into the vertical momentum equation. However, it is easier to rewrite the local acceleration and advection terms.

$$\frac{\partial \rho w}{\partial t} + \frac{\partial \rho w u}{\partial x} + \frac{\partial \rho w v}{\partial y} + \frac{\partial \rho w^2}{\partial z} = \rho \frac{\partial w}{\partial t} + \rho u \frac{\partial w}{\partial x} + \rho v \frac{\partial w}{\partial y} + .. \tag{B.15}$$

$$.. + \rho w \frac{\partial w}{\partial z} + w \frac{\partial \rho}{\partial t} + w \frac{\partial \rho u}{\partial x} + w \frac{\partial \rho v}{\partial y} + w \frac{\partial \rho w}{\partial z}$$

$$= \rho \frac{\partial w}{\partial t} + \rho u \frac{\partial w}{\partial x} + \rho v \frac{\partial w}{\partial y} + \rho w \frac{\partial w}{\partial z} \tag{B.16}$$

since $\frac{\partial \rho}{\partial t} + \frac{\partial \rho u}{\partial x} + \frac{\partial \rho v}{\partial y} + \frac{\partial \rho w}{\partial z} 0$.

$$\rho \frac{HU}{LT} \frac{\partial \tilde{w}}{\partial \tilde{t}} + \rho \frac{HU^2}{L^2} \tilde{u} \frac{\partial \tilde{w}}{\partial \tilde{x}} + \rho \frac{HU^2}{L^2} \tilde{v} \frac{\partial \tilde{w}}{\partial \tilde{y}} + \rho \frac{HU^2}{L^2} \tilde{w} \frac{\partial \tilde{w}}{\partial \tilde{z}} = -\frac{\partial p}{\partial z} - \rho g + \nu \rho \frac{HU}{L^3} \frac{\partial^2 \tilde{w}}{\partial \tilde{x}^2} + .. \tag{B.17}$$

$$.. + \nu \rho \frac{HU}{L^3} \frac{\partial^2 \tilde{w}}{\partial \tilde{y}^2} + \nu \rho \frac{U}{LH} \frac{\partial^2 \tilde{w}}{\partial \tilde{z}^2} + ..$$

$$.. + \nu \rho \frac{U}{LH} \frac{\partial^2 \tilde{u}}{\partial \tilde{x} \partial \tilde{z}} + \nu \rho \frac{U}{LH} \frac{\partial^2 \tilde{v}}{\partial \tilde{y} \partial \tilde{z}}$$

The only term that is not scaled is the pressure term, since it is not known what order this will be. Next, divide the equation by ρg.

$$\frac{HU}{LTg} \frac{\partial \tilde{w}}{\partial \tilde{t}} + \frac{HU^2}{gL^2} \tilde{u} \frac{\partial \tilde{w}}{\partial \tilde{x}} + \frac{HU^2}{gL^2} \tilde{v} \frac{\partial \tilde{w}}{\partial \tilde{y}} + \frac{HU^2}{gL^2} \tilde{w} \frac{\partial \tilde{w}}{\partial \tilde{z}} = -\frac{1}{\rho g} \frac{\partial p}{\partial z} - 1 + \nu \frac{HU}{gL^3} \frac{\partial^2 \tilde{w}}{\partial \tilde{x}^2} + .. \tag{B.18}$$

$$.. + \nu \frac{HU}{gL^3} \frac{\partial^2 \tilde{w}}{\partial \tilde{y}^2} + \nu \frac{U}{gLH} \frac{\partial^2 \tilde{w}}{\partial \tilde{z}^2} + ..$$

$$.. + \nu \frac{U}{gLH} \frac{\partial^2 \tilde{u}}{\partial \tilde{x} \partial \tilde{z}} + \nu \frac{U}{gLH} \frac{\partial^2 \tilde{v}}{\partial \tilde{y} \partial \tilde{z}}.$$

Notice that the stress gradient terms with second derivatives in the horizontal direction differ with a factor $(L/H)^2$ from the other stress gradient terms. Thus, these can be neglected. If $T = L/\sqrt{gH}$, then each factor in front of a term can be written as the following ratios

$$\begin{aligned} \text{local acceleration} \quad & \frac{FrH^2}{L^2} \\ \text{advective terms} \quad & \frac{Fr^2H^2}{L^2} \\ \text{stress gradients} \quad & \frac{Fr^2H}{ReL} \end{aligned} \tag{B.19}$$

where Fr is the Froude number and Re the Reynolds number.

$$Fr = \frac{U}{\sqrt{gH}}, \qquad Re = \frac{UH}{\nu} \tag{B.20}$$

B.3 Depth integration

The final step is to integrate Equations (3.13) and the continuity equation over the depth $h = \zeta - z_b$. The depth averaged values are defined as:

$$\bar{u} = \frac{1}{h}\int_{z_b}^{\zeta} u dz. \tag{B.21}$$

Integration of the continuity equation is given as follows,

$$\begin{aligned}\int_{z_b}^{\zeta} \frac{\partial u}{\partial x} + \frac{\partial v}{\partial y} + \frac{\partial w}{\partial z} dz =& \frac{\partial}{\partial x}\int_{z_b}^{\zeta} u dz - u^s\frac{\partial \zeta}{\partial x} + u^b\frac{\partial z_b}{\partial x} + \frac{\partial}{\partial y}\int_{z_b}^{\zeta} v dz - .. \\ &.. - v^s\frac{\partial \zeta}{\partial y} + v^b\frac{\partial z_b}{\partial y} + w^s - w^b \\ =& \frac{\partial \zeta}{\partial t} + \frac{\partial h\bar{u}}{\partial x} + \frac{\partial h\bar{v}}{\partial y} = 0\end{aligned} \tag{B.22}$$

where the Leibniz Integral Rule is used at the first line and boundary conditions (3.5) and (3.6) at the second line. Since the difference in momentum equations in $x-$ and $y-$direction are not that large, integration is only done for the $x-$direction. Integration of the Coriolis and pressure term is quite easy.

$$\int_{z_b}^{\zeta} f v dz = h f \bar{v} \tag{B.23}$$

$$\int_{z_b}^{\zeta} g\frac{\partial \zeta}{\partial x} dz = h\frac{\partial \bar{\zeta}}{\partial x} \tag{B.24}$$

Looking at the stress gradients, the same approach is used as for the continuity equation: using the Leibniz Integral Rule and then applying boundary conditions.

$$\begin{aligned}\int_{z_b}^{\zeta} \left(\frac{\partial \tau_{xx}}{\partial x} + \frac{\partial \tau_{xy}}{\partial y} + \frac{\partial \tau_{xz}}{\partial z}\right) dz =& \frac{\partial}{\partial x}\int_{z_b}^{\zeta} \tau_{xx} dz + \frac{\partial}{\partial y}\int_{z_b}^{\zeta} \tau_{xy} dz - .. \\ &.. - [\tau_{xx}\frac{\partial h}{\partial x} + \tau_{xy}\frac{\partial h}{\partial y} - \tau_{xz}]_{z=h} + [\tau_{xx}\frac{\partial z_b}{\partial x} + \tau_{xy}\frac{\partial z_b}{\partial y} - \tau_{xz}]_{z=z_b} \\ =& \frac{\partial \bar{\tau}_{xx} h}{\partial x} + \frac{\partial \bar{\tau}_{xy} h}{\partial y} + \tau_{wind,x} + \tau_{b,x}\end{aligned} \tag{B.25}$$

When integrating the local acceleration and advection terms it is a bit trickier. Also using the same approach as the continuity equation results in an expression that contains nonlinear terms.

$$\begin{aligned}\int_{z_b}^{\zeta}[\frac{\partial u}{\partial t}+\frac{\partial uu}{\partial x}+\frac{\partial uv}{\partial y}+\frac{\partial uw}{\partial z}]dz =& \frac{\partial}{\partial t}\int_{z_b}^{\zeta}udz+\frac{\partial}{\partial x}\int_{z_b}^{\zeta}uudz+\frac{\partial}{\partial y}\int_{z_b}^{\zeta}uvdz-.. \quad \text{(B.26)}\\ & .. - u^s\left(\frac{\partial\zeta}{\partial t}+u^s\frac{\partial\zeta}{\partial x}+v^s\frac{\partial\zeta}{\partial y}-w^s\right)+u^b\left(\frac{\partial z_b}{\partial t}+u^b\frac{\partial z_b}{\partial x}+v^b\frac{\partial z_b}{\partial y}-w^b\right)\\ =& \frac{\partial h\bar{u}}{\partial t}+\frac{\partial h\bar{u}\bar{u}}{\partial x}+\frac{\partial h\bar{u}\bar{v}}{\partial y}+..\\ & .. + \frac{\partial}{\partial x}\int_{z_b}^{\zeta}(u-\bar{u})^2dz+\frac{\partial}{\partial y}\int_{z_b}^{\zeta}(u-\bar{u})(v-\bar{v})dz\end{aligned}$$

where the boundary conditions are applied at the second line. Resulting shallow water equations can be found in Chapter 3.